IET The Institution of Engineering and Technology WILEY

ORIGINAL RESEARCH

Spatial multiplexing in near field MIMO channels with reconfigurable intelligent surfaces

Giulio Bartoli[1] ![ORCID] | Andrea Abrardo[1] | Nicolo Decarli[2] | Davide Dardari[3] | Marco Di Renzo[4] ![ORCID]

[1]University of Siena, Siena, Italy

[2]Italian Research Council, Bologna, Italy

[3]University of Bologna, Bologna, Italy

[4]Universite Paris-Saclay, CNRS, CentraleSupélec, Laboratoire des Signaux et Systèmes, Gif-sur-Yvette, France

Correspondence

Marco Di Renzo.
Email: marco.di-renzo@universite-paris-saclay.fr

Abstract

We consider a multiple-input multiple-output (MIMO) channel in the presence of a reconfigurable intelligent surface (RIS). Specifically, our focus is on analysing the spatial multiplexing gains in line-of-sight and low-scattering MIMO channels in the near field. We prove that the channel capacity is achieved by diagonalising the end-to-end transmitter-RIS-receiver channel, and applying the water-filling power allocation to the ordered product of the singular values of the transmitter-RIS and RIS-receiver channels. The obtained capacity-achieving solution requires an RIS with a non-diagonal matrix of reflection coefficients. Under the assumption of nearly-passive RIS, that is, no power amplification is needed at the RIS, the water-filling power allocation is necessary only at the transmitter. We refer to this design of RIS as a linear, nearly-passive, reconfigurable electromagnetic object (EMO). In addition, we introduce a closed-form and low-complexity design for RIS, whose matrix of reflection coefficients is diagonal with unit-modulus entries. The reflection coefficients are given by the product of two focusing functions: one steering the RIS-aided signal towards the mid-point of the MIMO transmitter and one steering the RIS-aided signal towards the mid-point of the MIMO receiver. We prove that this solution is exact in line-of-sight channels under the paraxial setup. With the aid of extensive numerical simulations in line-of-sight (free-space) channels, we show that the proposed approach offers performance (rate and degrees of freedom) close to that obtained by numerically solving non-convex optimization problems at a high computational complexity. Also, we show that it provides performance close to that achieved by the EMO (non-diagonal RIS) in most of the considered case studies.

KEYWORDS

MIMO communication, modulation

1 | INTRODUCTION

The need for terabits wireless links and sub-milliseconds (tactile) time responses in next-generation wireless systems, to support, for example, emerging augmented reality and virtual reality applications based on three-dimensional holographic video representations [1], exceeds the current capabilities of fifth-generation telecommunication standards. A possible solution to fulfil these requirements is the migration towards high frequency bands, notably the sub-terahertz and terahertz spectrum [2, 3]. The terahertz band offers, in fact, tens-hundreds gigahertz of contiguous bandwidth and enables the coexistence with other regulated spectra. Due to the large available bandwidth, the use of terahertz frequencies may extend the quality of experience of fibre-optic systems to wireless links, both in terms of data rates and time responses.

The use of terahertz signals for wireless communications is, however, challenging for several reasons, including the severe

propagation losses that drastically limit the communication coverage, and the lack of diffraction that makes wireless propagation occurs predominantly in line-of-sight [4]. Notably, it is shown in [5] that ensuring a strong line-of-sight connection is essential for fulfiling the desired communication performance. The severe path loss may be overcome and the availability of line-of-sight connections may be ensured with high probability through (a) a denser deployment of base stations (network densification); (b) the deployment of relays to split long-range transmission links into multiple short-range transmission links, possibly avoiding blocking objects; and (c) the use of highly-directive antenna arrays at the transmitter and receiver [6]. These solutions, however, usually result in an increase of backhaul infrastructure, power consumption, and hardware complexity [7]. Recent national and supranational directives have set, on the other hand, strict targets in reducing the energy consumption, such as the European Union that aims to reduce the power consumption by 32.5% before 2030 [8]. Recent activities within telecommunication standards organizations, for example, the third Generation Partnership Project (3GPP), in addition, are focused on the analysis of new network nodes to offer blanket coverage in cellular networks, in those scenarios where the deployment of full-stack cells may not always be possible (e.g., no availability of backhaul) or may not be economically viable [9].

In this context, two emerging technologies have recently gained major attention from the research community, and are suitable for enabling high rate, reduced hardware complexity, and high energy efficient communications, especially for transmission in the terahertz frequency band. The first technology is known as reconfigurable intelligent surface (RIS) [10, 11] and the second is known as holographic surface (HoloS) [12, 13]. Both technologies capitalize on recent progresses in the field of dynamic (reconfigurable) metasurfaces, even though they serve a different purpose and have different requirements [14]. An RIS is a relay-type surface whose main features are the low implementation complexity and the low power consumption, compared with conventional relay nodes, for example, decode-and-forward, amplify-and-forward, and the more recent network-controlled repeaters [15]. Specifically, an RIS is capable of shaping the electromagnetic waves with no power amplification and analog-to-digital conversion, which reduces the hardware complexity, power consumption, and processing delay (time response). A HoloS is, on the other hand, a hybrid continuous-aperture multiple-input multiple-output (MIMO) type transceiver [16], which is endowed with digital signal processing and power amplification capabilities, but with a reduced number of radio frequency chains compared to legacy MIMO implementations [17, 18]. Notably, two focused industry specification groups were recently established on terahertz communications and intelligent surfaces to coordinate the research efforts on these technologies and to strengthen their synergy and complementary [2, 19].

An RIS and a HoloS share the feature of being electrically-large, that is, their geometric size is much larger than the wavelength. This property makes them especially suitable for enabling spatial multiplexing in line-of-sight and low-scattering MIMO channels, which have been extensively studied in the past [20] and are currently receiving major renewed attention fueled by emerging potential applications and technology advances [21]. Specifically, two electrically large HoloS can support multimode transmission (spatial multiplexing) in line-of-sight channels, provided that the transmission range is within the radiative near field (Fresnel region) of each other [22–24]. Asymptotic analysis shows that the spatial multiplexing gain, that is, the number of degrees of freedom, is proportional to the product of the apertures of the HoloS and is inversely proportional to the square of the product of the wavelength and the transmission distance. The deployment of electrically-large HoloS at terahertz frequencies is, therefore, considered a suitable option to realize terabits wireless links with tactile time responses. The deployment of electrically-large RIS in such an environment is, likewise, considered an essential technology for ensuring reconfigurable short-range multi-hop links without requiring the deployment of large numbers of HoloS, thus fulfilling the requirements of blanket coverage at low cost and high energy efficiency, while preserving tactile time responses, since the signals are processed in the electromagnetic domain [6]. In addition, the deployment of RIS may enable spatial multiplexing gains in each line-of-sight hop, even though the line-of-sight direct link (between the transmit and receive HoloS) does not support spatial multiplexing, since operating in the far field [25, Section 7.2.5].

Despite the potential benefits of RIS-aided HoloS systems, especially in line-of-sight and low-scattering channels, the achievable spatial multiplexing gains and the optimal design for the precoding, decoding, and reflection coefficients of HoloS and RIS are an open problem. The available research works can be cast in two categories, as summarized in the next subsection.

1.1 | State of the art

The first category includes papers on the analysis and design of transmission links between two HoloS. The most relevant research works for this paper include [17, 22, 24, 26]. In [22], the author computes the number of degrees of freedom between two HoloS in the Fresnel region under the paraxial setup. In addition, the optimal precoding functions are given in a closed-form expression and are shown to be prolate spheroidal functions. In [24], the analysis in [22] is generalised to account for shorter transmission distances (or HoloS with a larger aperture). In [26], the authors consider non-paraxial setups and provide an approximated expression for the degrees of freedom and for the eigenfunctions, which are shown to be focusing functions. In [17], the authors propose and analyse a wavenumber-division multiplexing scheme to reduce the complexity of optimal spatial multiplexing schemes based on the prolate spheroidal functions identified in [22]. A more comprehensive overview, including recent works on line-of-sight MIMO, for example, [21] and references therein, can be found in [18]. None of these papers consider the presence of RIS.

In the rest of this paper, we model the transmit and receive HoloS as two critically-sampled MIMO arrays, that is, having antenna elements spaced by half-wavelength. This is in agreement with [16, 27], since the scope of this paper does not require to model the impact of surface waves [28]. Therefore, we refer to the considered system model as an RIS-aided MIMO channel.

The second category includes papers on the analysis and design of RIS-aided transmission links. The most relevant research works for this paper are those focused on MIMO arrays at the transmitter and the receiver, and include [29–36]. In [29], the authors optimise the RIS to maximise the spectral entropy (i.e., the effective rank) through a gradient-based interior-point method. In [30], the analysis in [29] is generalised for application to the multi-user setup. In [31], the authors propose an alternating optimization algorithm to find a locally optimal solution by iteratively optimising the transmit covariance matrix and the RIS reflection coefficients. In [32], the authors tackle a similar problem by proposing a more efficient numerical algorithm based on the projected gradient method. In [33], the authors consider an electromagnetically consistent model in the presence of mutual coupling (non-diagonal RIS matrices) and generalise the weighted minimum mean square error algorithm for application to multi-RIS MIMO interference channels. In [34], the authors focus on (pure) line-of-sight channels, and generalise the approach in [31] for application to double-RIS deployments. The algorithm is specialised for application to far-field MIMO channels, hence hampering spatial multiplexing gains greater than the number of RIS, that is, two. In [35], the authors introduce a numerical algorithm for jointly optimising the MIMO transmit precoder, the matrix of reflection coefficients of the RIS, and the MIMO receive equaliser, by minimising the data detection mean square error. In [36], the authors propose three numerical algorithms to maximise the sum-rate in RIS-aided MIMO broadcast channels. In all these papers, no closed-form expression for the matrix of reflection coefficients of the RIS is given, and all the algorithms are sub-optimal and are shown to be sensitive to the initialisation point and to the setup of the parameters for example, the step-size in gradient-based methods.

1.2 | Contributions

Based on the analysis of the state of the art, we evince that there is no contribution that characterises the optimal design of RIS-aided MIMO channels in terms of maximising the mutual information. Also, there is no contribution that provides a closed-form, even approximated, expression for the reflection coefficients of an RIS in line-of-sight and low-scattering channels.

Against this background, the main contribution of the present paper consists of (a) proving the optimal design of RIS that maximises the mutual information over general MIMO fading channels regardless of the implementation complexity, and (b) deriving a low-complexity design of RIS that is given in a closed-form expression and provides insights onto the achievable performance limits, especially for application to

line-of-sight MIMO channels at sub-terahertz and terahertz frequencies. Specifically, the present paper provides the following main contributions.

- In a general RIS-aided MIMO system, we prove that the channel capacity is achieved by diagonalising the end-to-end transmitter-RIS-receiver channel, and by applying the water-filling power allocation to the ordered product of the singular values of the (two individual) transmitter-RIS and RIS-receiver channels. The obtained capacity-achieving solution is shown to require an RIS with a non-diagonal matrix of reflection coefficients. Recently, non-diagonal RIS have been receiving increasing attention from the research community, since they can provide better performance at the expense of an increase of the hardware and implementation complexity, for example, [37–39]. To the best of the authors knowledge, however, no prior research work on non-diagonal RIS has proved the optimality of this architecture from an information-theoretic standpoint.[1] Under the assumption of nearly-passive RIS, that is, no power amplification is needed at the RIS, we prove that the water-filling power allocation is necessary only at the MIMO transmitter. We refer to this capacity-optimal RIS as a linear, nearly-passive, reconfigurable electromagnetic object (EMO).

- Even though an EMO is nearly-passive, that is, it does not require power amplifiers, and is capacity-achieving, it is characterised by a matrix of reflection coefficients with a non-diagonal structure. In general, all the entries of the matrix may be non-zero. This entails a non-negligible implementation complexity to realize the associated configuration network [37] or even the need of non-local designs [41, 42]. It is known, in addition, that RIS-aided systems characterised by non-diagonal matrices are more difficult to be optimised, in general [33]. Specifically, it is known that no closed-form solution for the optimal design of RIS is available in RIS-aided (pure) line-of-sight MIMO channels either [34]. As detailed in [34, Equation (5)], this is due to the non-convexity of the optimization problem and the coupling among the optimization variables (the matrix of reflection coefficients of the RIS and the precoding matrix at the MIMO transmitter). It is known, in addition, that the main computational complexity is due to the presence of the RIS, and that the existing optimization algorithms are computationally intensive, and are highly sensitive to the initialisation point and the free parameters of the algorithms (e.g., the step size) [36]. To overcome these difficulties, we introduce an approximated closed-form and low-complexity design for RIS, whose matrix of reflection coefficients is diagonal with unit-modulus entries. The reflection coefficients are given by the product of two focusing functions: one steering the RIS-aided signal towards the mid-point of the MIMO transmitter and one steering the RIS-aided signal towards the mid-point of the MIMO receiver. Notably, we prove that the proposed

---

[1]During the review process of the present paper, we have found [40], wherein the authors obtain a similar result.

solution is exact in (pure) line-of-sight channels under the paraxial setup [22].

- With the aid of extensive numerical simulations in line-of-sight (free-space) fading channels, we show that the proposed design for (diagonal) RIS offers performance (rate and degrees of freedom) close to that obtained by numerically solving non-convex optimization problems, which is known to entail a high computational complexity. Specifically, the numerical results unveil that the proposed solution works well even under non-paraxial setups, for which no analysis of the degrees of freedom and no closed-form expression of the channel eigenfunctions are available in closed-form for RIS-aided links [22, 26]. In addition, the numerical results show that the proposed approximated diagonal RIS offers performance very close to that of the EMO (with a non-diagonal structure), in several considered case studies. The proposed design can be considered as an approximate closed-form optimal solution for RIS-aided MIMO channels or a good-quality initial point for efficiently implementing currently-available non-convex optimization algorithms [31, 32]. Also, the proposed solution is applicable in every signal-to-noise-ratio regime, since the optimal precoding and decoding matrices at the MIMO transmitter and MIMO receiver are obtained by using conventional singular-value decomposition methods [43].

1.3 | Organization

The rest of this paper is organised as follows. In Section 2, we introduce the signal and system models. In Section 3, we characterise the capacity-achieving structure of RIS in general MIMO channels. In Section 4, we introduce a sub-optimal design for diagonal RIS, which is proved to be optimal in line-of-sight channels under the paraxial setup. In Section 5, we illustrate extensive simulation results over line-of-sight (free-space) channels, and non-paraxial system setups, to showcase the performance of the proposed closed-form sub-optimal design for RIS against state of the art numerical methods and the optimal EMO. In Section 6, conclusions are given.

2 | SIGNAL AND SYSTEM MODELS

We consider the communication system sketched in Figure 1, where a MIMO transmitter, for example, a base station (BS), communicates with a MIMO receiver, for example, a user equipment (UE), with the aid of an RIS. The transmitter and the receiver are equipped with N and M antennas, respectively. The RIS is modelled as a MIMO array compromising K reconfigurable scattering elements. As discussed in Section 1, the antennas at the transmitter and receiver, and the reconfigurable elements at the RIS are assumed to be critically spaced at half-wavelength.

The channel matrix between the transmitter and the RIS is denoted by $\mathbf{H}_F \in \mathbb{C}^{K \times N}$ (forward channel), and the channel matrix between the RIS and the receiver is denoted by $\mathbf{H}_B \in \mathbb{C}^{M \times K}$ (backward or scattered channel). No specific assumptions about the characteristics of the channels are made, even though the focus of this paper is on analysing the multiplexing gain of the considered RIS-aided MIMO system in line-of-sight and low-scattering channels, where no spatial multiplexing gain can be obtained in the far field [25].

The end-to-end (transmitter-RIS-receiver) MIMO channel can be formulated as

$$\mathbf{H} = \mathbf{H}_B \boldsymbol{\Phi} \mathbf{H}_F \tag{1}$$

where $\boldsymbol{\Phi}$ denotes the $K \times K$ matrix of reflection coefficients of the RIS.

Typical designs for RIS assume that the matrix of reflection coefficients $\boldsymbol{\Phi}$ is diagonal with unit-modulus entries [39]. This design eases the implementation complexity of RIS, but may not necessarily be optimal from the point of view of the power efficiency [41, 42], performance [37], or may not consider the impact of mutual coupling in sub-wavelength (with
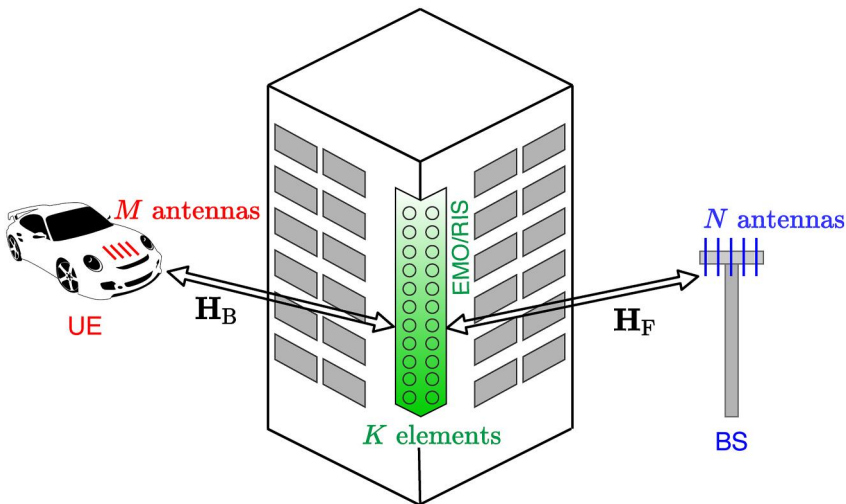

FIGURE 1 Considered scenario: A MIMO transmitter (a BS) communicates with a MIMO receiver (a UE) with the aid of an RIS.

inter-distances less than half-wavelength) implementations [44]. Collectively, as mentioned in Section 1, these designs fall within the umbrella of non-diagonal RIS. However, there exist no information-theoretic studies that quantify the optimality of non-diagonal RIS compared with diagonal RIS.

To shed light on the optimal design of RIS from an information-theoretic standpoint, we depart by considering an arbitrary structure for the matrix $\boldsymbol{\Phi}$, which is not necessarily diagonal. The only imposed constraint for $\boldsymbol{\Phi}$ is to be a unitary matrix, that is, $\boldsymbol{\Phi}\boldsymbol{\Phi}^\dagger = \mathbf{I}_K$, where $(\cdot)^\dagger$ is the Hermitian adjoint operator and $\mathbf{I}_K$ is the $K \times K$ identity matrix. The assumption of unitary matrix ensures that the RIS does not amplify the incident signals but relaxes the assumption of diagonal structure. This will be apparent in the next sections.

An RIS with a non-diagonal unitary matrix $\boldsymbol{\Phi}$ is referred to as an EMO with the following characteristics.

- It is a noise-less device, as opposed to non-regenerative relays [7];
- It is a linear device whose output signals are linear combinations of the input signals;
- It is reconfigurable, that is, the matrix $\boldsymbol{\Phi}$ can be optimised as desired;
- It is nearly-passive, that is, it does not amplify the incident signals thanks to the design constraint $\boldsymbol{\Phi}\boldsymbol{\Phi}^\dagger = \mathbf{I}_K$. A formal proof for this statement is given in the next section.

To facilitate the analysis, the forward and backward channels can be formulated by invoking the singular-value decomposition (SVD) applied to $\mathbf{H}_F$ and $\mathbf{H}_B$. Specifically, let diag$\{v_1, v_2, \ldots\}$ denote a general rectangular matrix whose main diagonal has elements given by $v_1, v_2, \cdots$, and let σ_{Fi} and σ_{Bi} denote the N and M (non-zero and zero) ordered singular values of $\mathbf{H}_F$ and $\mathbf{H}_B$, respectively. For simplicity, we assume $N < K$ and $M < K$. Also, let $N_F \leq N$ and $M_B \leq M$ be the numbers of non-zero singular values of $\mathbf{H}_F$ and $\mathbf{H}_B$, respectively. Then, we introduce the following matrices.

$$\boldsymbol{\Sigma}_F = \text{diag}\{\sigma_{F1}, \ldots, \sigma_{FN}\} \in \mathbb{C}^{K \times N} \quad (2)$$

$$\boldsymbol{\Sigma}_B = \text{diag}\{\sigma_{B1}, \ldots, \sigma_{BM}\} \in \mathbb{C}^{M \times K} \quad (3)$$

In addition, let $\mathbf{U}_F \in \mathbb{C}^{K \times K}$, $\mathbf{V}_F \in \mathbb{C}^{N \times N}$, $\mathbf{U}_B \in \mathbb{C}^{M \times M}$, and $\mathbf{V}_B \in \mathbb{C}^{K \times K}$ be unitary matrices fulfilling the following equalities.

$$\mathbf{H}_F = \mathbf{U}_F \boldsymbol{\Sigma}_F \mathbf{V}_F^\dagger \quad (4)$$

$$\mathbf{H}_B = \mathbf{U}_B \boldsymbol{\Sigma}_B \mathbf{V}_B^\dagger \quad (5)$$

Therefore, the end-to-end channel $\mathbf{H}$ can be expressed as

$$\mathbf{H} = \mathbf{H}_B \boldsymbol{\Phi} \mathbf{H}_F = \mathbf{U}_B \boldsymbol{\Sigma}_B \mathbf{V}_B^\dagger \boldsymbol{\Phi} \mathbf{U}_F \boldsymbol{\Sigma}_F \mathbf{V}_F^\dagger \quad (6)$$

By definition, the maximum number of communication modes (i.e., the channel degrees of freedom) is $\text{DoF}_{\max} = \min (N_F, M_B)$. The actual number of degrees of freedom highly depends on the properties of the channels $\mathbf{H}_F$ and $\mathbf{H}_B$, and on the matrix $\boldsymbol{\Phi}$ of the RIS reflection coefficients. The objective of this paper is to optimise the matrix $\boldsymbol{\Phi}$ in order to maximise the end-to-end channel capacity given the channels $\mathbf{H}_F$ and $\mathbf{H}_B$.

3 | CAPACITY-ACHIEVING MATRIX OF REFLECTION COEFFICIENTS

In this section, we identify the optimal structure for the unitary matrix $\boldsymbol{\Phi}$ that is capacity-achieving. The received signal $\mathbf{y} \in \mathbb{C}^M$ is

$$\mathbf{y} = \mathbf{H}\mathbf{x} + \mathbf{n} \quad (7)$$

where $\mathbf{x} \in \mathbb{C}^N$ is the transmitted signal, $\mathbf{n} \in \mathbb{C}^M$ is the additive white Gaussian noise (AWGN) with $\mathbf{n} \sim \mathcal{CN}\left(\mathbf{0}, \sigma_n^2 \mathbf{I}_M\right)$, where σ_n^2 is the noise power and $\mathcal{CN}(\cdot, \cdot)$ denotes a multivariate complex Normal distribution.

Also, let $\mathbf{Q}$ be the positive semi-definite (i.e., $\mathbf{Q} \succeq 0$) covariance matrix of the transmitted signal, that is, $\mathbb{E}[\mathbf{x}\mathbf{x}^\dagger] = \mathbf{Q}$, where $\mathbb{E}[\cdot]$ is the expectation operator. Then, the transmit power constraint is $\text{tr}(\mathbf{Q}) \leq P$, where $\text{tr}(\cdot)$ is the trace operator and P is the total transmit power.

According to [25], the channel capacity is obtained by maximising the mutual information between the transmitted and received symbols as a function of $\mathbf{Q}$ and $\boldsymbol{\Phi}$

$$C = \max_{\substack{\mathbf{Q} \succeq 0, \text{tr}(\mathbf{Q}) \leq P \\ \boldsymbol{\Phi}\boldsymbol{\Phi}^\dagger = \mathbf{I}_K}} I(\mathbf{x}, \mathbf{y}) = \log \det\left(\mathbf{I}_M + \frac{1}{\sigma_n^2} \mathbf{H}\mathbf{Q}\mathbf{H}^\dagger\right) \quad (8)$$

where $\det(\cdot)$ is the determinant of a square matrix.

The channel capacity in Equation (8) and how to achieve it are given in the following proposition.

Proposition 1 *The end-to-end channel capacity in* Equation (8) *is*

$$C = \sum_{i=1}^{\min\{N_F, M_B\}} \log\left(1 + \sigma_{Fi}^2 \sigma_{Bi}^2 \frac{P_i}{\sigma_n^2}\right) \quad (9)$$

where $P_i = \left(\mu - \frac{\sigma_n^2}{\sigma_{Fi}^2 \sigma_{Bi}^2}\right)^+ = \max\left(0, \mu - \frac{\sigma_n^2}{\sigma_{Fi}^2 \sigma_{Bi}^2}\right)$ *and* μ *is obtained by fulfiling the identity* $\sum_{i=1}^{\min\{N_F, M_B\}} P_i = P$. *In addition,* C *is attained by setting.*

$$l\mathbf{Q} = \mathbf{V}_F \text{diag}\{P_1, P_2, \ldots\} \mathbf{V}_F^\dagger \quad (10)$$

$$\boldsymbol{\Phi} = \mathbf{V}_B \mathbf{U}_F^\dagger \quad (11)$$

Proof See Appendix A. □

Based on Proposition 1, the following comments are in order.

- The capacity in Equation (9) generalises the capacity for MIMO channels in [25], by considering the impact of an EMO (the optimal non-diagonal unitary RIS). Similar to [25], the end-to-end channel capacity is attained by diagonalising the end-to-end transmitter-RIS-receiver channel, and by applying the water-filling power allocation to the ordered product of the singular values of the transmitter-RIS and RIS-receiver channels taken individually.

- The capacity in Equation (9) holds true for any channel models (i.e., regardless of the fading distribution and the carrier frequency), and offers a simple closed-form solution for the optimal covariance matrix at the transmitter and the optimal design for the RIS. This is in stark contrast with computationally intensive algorithms that are typically utilised for optimising diagonal and non-diagonal RIS, for example, [34, 36, 39].

- An RIS with a diagonal matrix $\boldsymbol{\Phi}$ of unit-modulus reflection coefficients is, in general, not capacity-achieving. An RIS with a non-diagonal unitary matrix $\boldsymbol{\Phi}$ may be, on the other hand, capacity-achieving. Also, the optimal design is available in a closed-form expression based on the SVD decomposition of the transmitter-RIS and RIS-receiver channels.

- By direct inspection of Equation (9), it is apparent that considering a non-diagonal but unitary matrix $\boldsymbol{\Phi}$ is sufficient for ensuring that the RIS does not result in any power amplification, thus making the EMO a nearly-passive device like a diagonal RIS.

- Similar to [25], the capacity in Equation (9) holds true for any operating signal-to-noise ratio.

- The formula in Equation (9) resembles the capacity of non-regenerative relays [45, 46]. The main differences between the EMO and a non-regenerative relay are that the former is noise-free and no power allocation at the EMO is needed, since it is characterised by a unitary matrix. This makes the proof of Proposition 1 different from [45, 46], since there is no need to apply a whitening matrix. Due to the capability of non-regenerative relays to amplify the received signal, the optimal power allocation strategy is known, in a closed-form expression, only if the transmitter applies an equal power allocation strategy [46]. Otherwise, the optimal power allocation needs to be computed by solving an optimization algorithm. The optimal power allocation at the MIMO transmitter and the optimal matrix of the RIS reflection coefficients are, on the other hand, formulated in closed-form expressions in Proposition 1.

Proposition 1 unveils that the optimal design for RIS with a unitary matrix of reflection coefficients is non-diagonal. Non-diagonal RIS have attracted recent interest in the literature, and, supported by Proposition 1, they usually outperform diagonal RIS [39]. However, their practical implementation is more difficult, especially due to the complex configuration network to realize non-diagonal

matrices. Based on the optimal design for unitary RIS in Equation (11), it is, however, possible to investigate approximated diagonal (hence unitary by definition) designs for RIS that provide a rate close to the end-to-end channel capacity in Equation (9). This is discussed next.

4 | PROPOSED DESIGN FOR NEARLY-OPTIMAL DIAGONAL RIS

In this section, we propose an approximated design for RIS whose matrix of reflection coefficients is diagonal, and analyse the conditions under which it is either optimal or nearly-optimal. As a criterion of optimality, we consider the end-to-end channel capacity in Proposition 1. In other words, a diagonal RIS is deemed optimal if the resulting end-to-end transmitter-RIS-receiver channel can be diagonalised and the capacity in Equation (9) is attained. For the avoidance of doubt, the diagonal matrix of reflection coefficients of the RIS is denoted by $\tilde{\boldsymbol{\Phi}}$.

Without loss of generality, we assume that the $K \times K$ diagonal matrix $\tilde{\boldsymbol{\Phi}}$ is given by the product of 2 $K \times K$ diagonal matrices $\mathbf{F}_{RB}$ and $\mathbf{F}_{RF}$, as follows

$$\tilde{\boldsymbol{\Phi}} = \mathbf{F}_{RB}\mathbf{F}_{RF}^{\dagger} \tag{12}$$

The definition and meaning of $\mathbf{F}_{RB}$ and $\mathbf{F}_{RF}$ based on the considered criterion of optimality are given next. Furthermore, let us express the unitary matrices $\mathbf{V}_F \in \mathbb{C}^{N \times N}$, $\mathbf{U}_F \in \mathbb{C}^{K \times K}$, $\mathbf{V}_B \in \mathbb{C}^{K \times K}$, and $\mathbf{U}_B \in \mathbb{C}^{M \times M}$ in Equations (4) and (5), as follows.

$$\mathbf{V}_F = \mathbf{F}_T\mathbf{P}_T \in \mathbb{C}^{N \times N} \tag{13}$$

$$\mathbf{U}_F = \mathbf{F}_{RF}\mathbf{P}_{RF} \in \mathbb{C}^{K \times K} \tag{14}$$

$$\mathbf{V}_B = \mathbf{F}_{RB}\mathbf{P}_{RB} \in \mathbb{C}^{K \times K} \tag{15}$$

$$\mathbf{U}_B = \mathbf{F}_R\mathbf{P}_R \in \mathbb{C}^{M \times M} \tag{16}$$

where $\mathbf{F}_T$ and $\mathbf{F}_R$ are $N \times N$ and $M \times M$ diagonal matrices, respectively, $\mathbf{P}_T$ and $\mathbf{P}_R$ are $N \times N$ and $M \times M$ non-diagonal unitary matrices, respectively, and $\mathbf{P}_{RF}$ and $\mathbf{P}_{RB}$ are $K \times K$ non-diagonal unitary matrices. The analytical formulation in Equations (13)–(16) holds, without loss of generality, for any choice of the diagonal matrices $\mathbf{F}_{RB}$ and $\mathbf{F}_{RF}$ in Equation (12), and for any channels $\mathbf{H}_F$ and $\mathbf{H}_B$, by appropriately choosing the non-diagonal unitary matrices $\mathbf{P}_T$, $\mathbf{P}_R$, $\mathbf{P}_{RF}$, and $\mathbf{P}_{RB}$.

Based on these definitions, the end-to-end channel in Equation (6) can be reformulated as

$$\begin{aligned}
\mathbf{H} = \mathbf{H}_B\tilde{\boldsymbol{\Phi}}\mathbf{H}_F &= \left(\mathbf{F}_R\mathbf{P}_R\boldsymbol{\Sigma}_B\mathbf{P}_{RB}^{\dagger}\mathbf{F}_{RB}^{\dagger}\right)\left(\mathbf{F}_{RB}\mathbf{F}_{RF}^{\dagger}\right) \\
&\times \left(\mathbf{F}_{RF}\mathbf{P}_{RF}\boldsymbol{\Sigma}_F\mathbf{P}_T^{\dagger}\mathbf{F}_T^{\dagger}\right)
\end{aligned} \tag{17}$$

Since $\mathbf{F}_{RB}^{\dagger}\mathbf{F}_{RB} = \mathbf{I}_K$ and $\mathbf{F}_{RF}^{\dagger}\mathbf{F}_{RF} = \mathbf{I}_K$, we obtain

$$\mathbf{H} = \left(\mathbf{F}_R\mathbf{P}_R\boldsymbol{\Sigma}_B\right)\left(\mathbf{P}_{RB}^{\dagger}\mathbf{P}_{RF}\right)\left(\boldsymbol{\Sigma}_F\mathbf{P}_T^{\dagger}\mathbf{F}_T^{\dagger}\right) \qquad (18)$$

Since, by definition, $\mathbf{U}_B = \mathbf{F}_R\mathbf{P}_R$ and $\mathbf{V}_F^{\dagger} = \mathbf{P}_T^{\dagger}\mathbf{F}_T^{\dagger}$, we obtain

$$\mathbf{H} = \left(\mathbf{U}_B\boldsymbol{\Sigma}_B\right)\left(\mathbf{P}_{RB}^{\dagger}\mathbf{P}_{RF}\right)\left(\boldsymbol{\Sigma}_F\mathbf{V}_F^{\dagger}\right) \qquad (19)$$

From Proposition 1, the end-to-end channel capacity in Equation (9) is obtained by diagonalising the transmitter-RIS-receiver channel, as follows

$$\mathbf{H}_{diag} = \mathbf{H}_B\left(\mathbf{V}_B\mathbf{U}_F^{\dagger}\right)\mathbf{H}_F = \mathbf{U}_B\boldsymbol{\Sigma}_B\boldsymbol{\Sigma}_F\mathbf{V}_F^{\dagger} = \mathbf{U}_B\boldsymbol{\Gamma}\mathbf{V}_F^{\dagger} \qquad (20)$$

where $\boldsymbol{\Gamma} = \boldsymbol{\Sigma}_B\boldsymbol{\Sigma}_F \in \mathbb{C}^{M \times N}$ is an $M \times N$ diagonal matrix.

By comparing Equations (19) and (20), we evince that a diagonal RIS is optimal from the end-to-end channel capacity standpoint if $\mathbf{P}_{RB}^{\dagger}\mathbf{P}_{RF} = \mathbf{I}_K$, since the end-to-end channel is diagonalised according to Proposition 1, that is, $\mathbf{H} = \mathbf{H}_{diag}$. In other words, a diagonal RIS would be nearly-optimal, from the end-to-end channel capacity standpoint, in all setups in which $\mathbf{H} \approx \mathbf{H}_{diag}$. This provides a simple criterion for optimising the matrix $\boldsymbol{\Phi}$, while ensuring a low-complexity implementation (i.e., a diagonal structure) and near-optimality based on Proposition 1. Therefore, several designs for RIS may be conceived, offering the desired tradeoff between achievable rate and implementation complexity, in contrast to fully-connected non-diagonal RIS [39].

Based on the design criterion $\mathbf{H} \approx \mathbf{H}_{diag}$ for optimising the diagonal matrix $\tilde{\boldsymbol{\Phi}}$, it is worth analysing whether there exist channel models and setups under which a diagonal RIS is strictly optimal, that is, $\mathbf{H} = \mathbf{H}_{diag}$. In addition, it is worth analysing whether approximated closed-form expressions for $\tilde{\boldsymbol{\Phi}}$ that fulfil the condition $\mathbf{H} \approx \mathbf{H}_{diag}$ can be identified, especially in line-of-sight or low-scattering channels. These aspects are discussed in the next two sub-sections.

4.1 | Line-of-sight channels and paraxial setup

A known and important case study in which a diagonal RIS is strictly optimal, that is, $\mathbf{H} = \mathbf{H}_{diag}$, is sketched in Figure 2 for, without loss of generality, linear arrays [23]. Specifically, the scenario in Figure 2 is representative of a refracting RIS, enabling, for example outdoor-to-indoor or room-to-room communications [47]. We consider (pure) line-of-sight channels where the MIMO transmitter, the RIS, and the MIMO receiver are in the near field of each other (Fresnel region), the mid-points of the transmitter, RIS, and receiver are perfectly aligned, and the MIMO transmitter and MIMO receiver are located on the opposite sides of the RIS. This network topology is usually referred to as the paraxial setup [22]. Also, we assume that the distance between the mid-points of the MIMO transmitter and the RIS (d_F in Figure 2), and the distance between the mid-points of the RIS and the MIMO receiver (d_B in Figure 2) are the same, that is, $d_F = d_B$, and $N = M$. In detail, the line-of-sight transmitter-RIS and RIS-receiver links are denoted by $\mathbf{H}_F = \left\{h_{nk}^{(F)}\right\}$ and $\mathbf{H}_B = \left\{h_{km}^{(B)}\right\}$, and the channel gains are given by.

$$h_{nk}^{(F)} = \frac{1}{4\pi d_{nk}^{(F)}}e^{J\kappa d_{nk}^{(F)}} \qquad (21)$$

$$h_{km}^{(B)} = \frac{1}{4\pi d_{km}^{(B)}}e^{J\kappa d_{km}^{(B)}} \qquad (22)$$

where $d_{nk}^{(F)}$ is the distance between the nth antenna of the MIMO transmitter and the kth element of the RIS, $d_{km}^{(B)}$ is the distance between the kth element of the RIS and the mth antenna of the MIMO receiver, J is the imaginary unit, and $\kappa = 2\pi/\lambda$ with λ being the wavelength.

Under these conditions, it is known from [22] (for surfaces or planar antenna arrays) and [23] (for lines or linear arrays) that $\mathbf{P}_{RB}^{\dagger}\mathbf{P}_{RF} = \mathbf{I}_K$, and, notably, the matrices $\mathbf{P}_{RB}$ and $\mathbf{P}_{RF}$ are obtained by spatially sampling, at half-wavelength, prolate
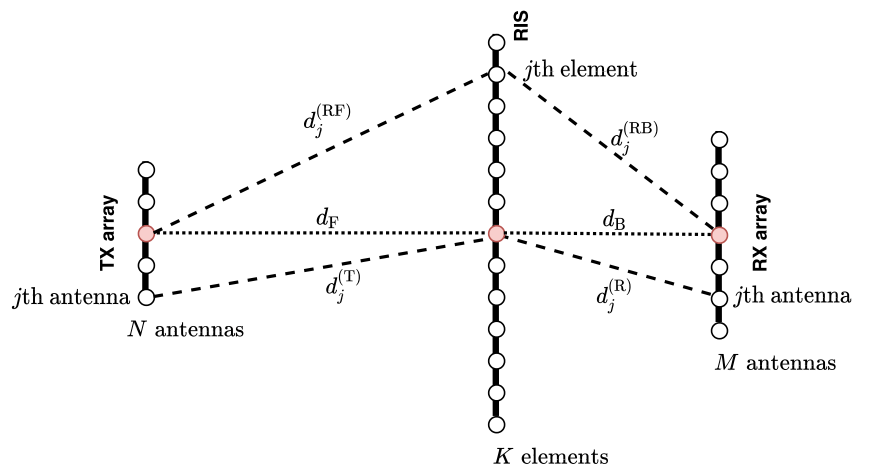

FIGURE 2 Example of deployment scenario in which a diagonal RIS is optimal from the capacity standpoint: Line-of-sight channels and paraxial setup.

spheroidal functions [48]. In addition, the diagonal matrix $\tilde{\boldsymbol{\Phi}} = \mathbf{F}_{RB}\mathbf{F}_{RF}^{\dagger}$ is available in a closed-form expression, as.

$$\mathbf{F}_{RF} = \text{diag}\left\{e^{\jmath\kappa d_1^{(RF)}}, \ldots, e^{\jmath\kappa d_K^{(RF)}}\right\} \in \mathbb{C}^{K \times K} \quad (23)$$

$$\mathbf{F}_{RB} = \text{diag}\left\{e^{-\jmath\kappa d_1^{(RB)}}, \ldots, e^{-\jmath\kappa d_K^{(RB)}}\right\} \in \mathbb{C}^{K \times K} \quad (24)$$

where, as illustrated in Figure 2, $d_j^{(RF)}$ is the distance between the mid-point of the MIMO transmitter and the jth element of the RIS, and $d_j^{(RB)}$ is the distance between the jth element of the RIS and the mid-point of the MIMO receiver. In [22], the functions in Equations (23) and (24) are referred to as focusing functions. In this scenario, in addition, the functions $\mathbf{F}_T$, $\mathbf{F}_T$, $\mathbf{P}_T$, and $\mathbf{P}_R$ in Equation (13) and (16) can be computed analogously, as elaborated in [22].

4.2 | Approximated closed-form expression for $\tilde{\boldsymbol{\Phi}} = \mathbf{F}_{RB}\mathbf{F}_{RF}^{\dagger}$

The case study analysed in the previous section is a very special setup. However, it is instrumental to motivate the proposed approximated design for $\tilde{\boldsymbol{\Phi}} = \mathbf{F}_{RB}\mathbf{F}_{RF}^{\dagger}$. Based on recent results, that is, [49, 50], it is considered difficult to optimise an RIS based on instantaneous channel state information, for example, based on estimates of $\mathbf{H}_F$ and $\mathbf{H}_B$ that account for the impact of small-scale fading. This is due to the associated large pilot overhead, which typically grows with the product of the number of RIS elements (K) and the number of users in the network. A more pragmatic choice is to optimise the RIS based on long-term channel statistics, for example, the locations of the transmitter, RIS, and receiver, ignoring the small-scale fading. On the other hand, the MIMO transmitter and MIMO receiver are optimised based on full channel state information, similar to legacy systems, once the RIS is optimised. The focusing functions in Equations (23) and (24) are optimal in line-of-sight channels and the RIS is optimised based only on the transmission distances. Under non-paraxial setups, the identity $\mathbf{P}_{RB}^{\dagger}\mathbf{P}_{RF} = \mathbf{I}_K$ is, however, never exactly fulfiled, since $\mathbf{P}_{RB} \neq \mathbf{P}_{RF}$ in general. However, for any arbitrary matrix $\tilde{\boldsymbol{\Phi}}$, the numerical computation of $\mathbf{P}_{RF}$ and $\mathbf{P}_{RB}$ is known to be straightforward [34], since, as apparent from Equations (14) and (15), it can be obtained by simply computing the SVD of the channels $\mathbf{H}_F$ and $\mathbf{H}_B$, respectively. The numerical computation of $\mathbf{P}_{RF}$ and $\mathbf{P}_{RB}$ can, in addition, partially compensate for any sub-optimality arising from the approximated choice for $\mathbf{F}_{RF}$ and $\mathbf{F}_{RB}$ in non-paraxial setups.

Based on these considerations, we propose the following approximated design for $\tilde{\boldsymbol{\Phi}}$.

- Regardless of the channel model and the network topology, the diagonal matrix of reflection coefficients of the RIS is set equal to $\tilde{\boldsymbol{\Phi}} = \mathbf{F}_{RB}\mathbf{F}_{RF}^{\dagger}$, with $\mathbf{F}_{RF}$ and $\mathbf{F}_{RB}$ given in Equations (23) and (24), respectively.

- Given $\tilde{\boldsymbol{\Phi}}$, the precoding and decoding matrices at the MIMO transmitter and MIMO receiver, respectively, are obtained by applying the SVD to the end-to-end transmitter-RIS-receiver channel $\mathbf{H} = \mathbf{H}_B\tilde{\boldsymbol{\Phi}}\mathbf{H}_F = \mathbf{H}_B\mathbf{F}_{RB}\mathbf{F}_{RF}^{\dagger}\mathbf{H}_F$ [43].

We expect that the proposed approximated design for $\tilde{\boldsymbol{\Phi}}$ is sufficiently accurate in line-of-sight and low-scattering channels, for example, for application in the millimetre-wave, sub-terahertz, and terahertz frequency bands, and the location of the RIS is optimised in order to maximise the end-to-end performance given the locations of the MIMO transmitter and MIMO receiver. However, the proposed diagonal design for $\tilde{\boldsymbol{\Phi}}$ can be applied to any channel models, under the assumption that the RIS is optimised based on position information rather than on instantaneous channel state information, which may be difficult to obtain in RIS-aided channels [49]. The optimality, from the end-to-end channel capacity standpoint, of the proposed approximated diagonal design is analysed, with the aid of extensive numerical simulations, in the next section. Specifically, the rate obtained with the proposed design is compared against currently available numerical methods that jointly optimise the transmitter, the diagonal RIS, and the receiver [49], as well as the EMO (non-diagonal RIS) based on Proposition 1.

5 | NUMERICAL RESULTS

In this section, we analyse the effectiveness of the proposed closed-form expression for diagonal RIS with the aid of numerical simulations. Specifically, we compare the rate obtained by three schemes.

- The EMO in Proposition 1, which is the optimal capacity-achieving non-diagonal design for RIS that is obtained as the solution of Equation (8). The capacity of this scheme is given by Equation (9) without the need of solving any non-convex optimization problems. Only the SVD of the two channels $\mathbf{H}_F$ and $\mathbf{H}_B$ needs to be computed. This scheme is denoted as "Non-diagonal RIS" (ND-RIS) in the figures.

- The conventional joint optimization of the covariance matrix of the transmitted symbols and the diagonal matrix of the RIS, by numerically solving the following non-convex optimization problem

$$\begin{array}{c}\max\limits_{\substack{\mathbf{Q}\succ 0, \text{tr}(\mathbf{Q})\leq P \\ |\boldsymbol{\Phi}(k,k)|=1, \angle\boldsymbol{\Phi}(k,k)\in[0,2\pi), \boldsymbol{\Phi}(k,h\neq k)=0}} \\ \times \log\det\left(\mathbf{I}_M + \frac{1}{\sigma_n^2}(\mathbf{H}_B\boldsymbol{\Phi}\mathbf{H}_F)\mathbf{Q}(\mathbf{H}_B\boldsymbol{\Phi}\mathbf{H}_F)^{\dagger}\right)\end{array} \quad (25)$$

where $|a|$ and $\angle a$ denote the absolute value and the phase of a, respectively. In this case, the algorithm in [49] is utilised. This scheme is denoted as "Diagonal RIS - Numerical" (D-RIS-NUM) in the figures.

- The proposed approximated design for RIS, according to which the diagonal matrix of the RIS reflection coefficients is $\mathbf{\Phi} = \tilde{\mathbf{\Phi}} = \mathbf{F}_{RB}\mathbf{F}_{RF}^{\dagger}$ with $\mathbf{F}_{RF}$ and $\mathbf{F}_{RB}$ given in Equations (23) and (24), respectively, and the covariance matrix of the transmitted symbols is the solution of the following convex optimization problem

$$\max_{\mathbf{Q}>0,\mathrm{tr}(\mathbf{Q})\leq P} \log \det$$

$$\times \left(\mathbf{I}_M + \frac{1}{\sigma_n^2}\left(\mathbf{H}_{\mathbf{B}}\left(\mathbf{F}_{RB}\mathbf{F}_{RF}^{\dagger}\right)\mathbf{H}_{\mathbf{F}}\right)\mathbf{Q}\left(\mathbf{H}_{\mathbf{B}}\left(\mathbf{F}_{RB}\mathbf{F}_{RF}^{\dagger}\right)\mathbf{H}_{\mathbf{F}}\right)^{\dagger}\right)$$

(26)

whose solution is known to be the water-filling power allocation applied to the end-to-end channel, considering $\mathbf{\Phi} = \tilde{\mathbf{\Phi}} = \mathbf{F}_{RB}\mathbf{F}_{RF}^{\dagger}$ fixed [43]. This scheme is denoted as "Diagonal RIS - Proposed" (D-RIS-FOC) in the figures. In particular, the focusing functions in (23) and (24) assume, unless stated otherwise, that the focusing points are the midpoints of the MIMO transmitter and MIMO receiver, respectively. To analyse the sensitivity of the proposed solution, we analyse the impact of considering focusing points different from the mid-points of the MIMO transmitter and MIMO receiver as well. For generality, we use the notation $\mathbf{\Phi} = \tilde{\mathbf{\Phi}} = \mathbf{F}_{RB}(\mathbf{p}_{RB})\mathbf{F}_{RF}(\mathbf{p}_{RF})^{\dagger}$, where $\mathbf{p}_{RF}$ is the focusing point at the MIMO transmitter and $\mathbf{p}_{RB}$ is the focusing point the MIMO receiver.

The considered network topology is illustrated in Figure 3. The mid-points of the MIMO transmitter, RIS, and MIMO receiver are denoted by $\mathbf{c}_B$, $\mathbf{c}_R$, $\mathbf{c}_U$, respectively, and they lay on the $z = 0$ plane. The distances between the mid-points of the MIMO transmitter and the RIS, and the mid-points of the RIS and the MIMO receiver are denoted by d_F and d_B, respectively. The angles between the lines connecting the mid-points of the MIMO transmitter and the RIS, and the mid-points of the RIS and the MIMO receiver and the normal to the RIS are denoted by θ_F and θ_B, respectively. Also, the angles between the MIMO transmitter and the z-axis and between the MIMO receiver and the z-axis are denoted by ψ_F and ψ_B, respectively. The RIS is always kept parallel to the yz plane. Therefore, the MIMO transmitter, RIS, and MIMO receiver are parallel to each other if $\psi_F = \psi_B = 0$.

To validate the proposed design, the line-of-sight (free-space) channel model in Equations (21) and (22) is utilised. Similar results for transmission over Rician fading channels can be found in [51]. Regardless of the channel model being used, however, it is worth noting that the ND-RIS and D-RIS-NUM schemes require instantaneous channel state information to operate. The D-RIS-FOC scheme, on the other hand, only requires information on the positions of the transmitter, receiver, and unit cells of the RIS [49]. Readers interested in channel estimation for RIS-aided channels are referred to [50] for an extensive overview and for the available algorithms and protocols. Unless stated otherwise, the numerical results are obtained by assuming a carrier frequency of 28 GHz. The MIMO transmitter comprises $N = 32$ antennas (8 along the y-axis and 4 along the z axis), the RIS comprises $K = 1024$ elements (512 along the y-axis and 2 along the z axis), and the MIMO receiver comprises $M = 16$ antennas (16 along the y-axis and 1 along the z axis). The noise variance is set to $\sigma_n^2 = -97$ dBm and the total transmit power is set to $p = 0$ dBm. The inter-distance of the antenna elements at the MIMO transmitter, MIMO receiver, and at the RIS is equal to half-wavelength.

5.1 | Paraxial setup

In this sub-section, we compare the achievable rate between the "Diagonal RIS - Numerical" (D-RIS-NUM) and "Diagonal RIS - Proposed" (D-RIS-FOC) schemes in the paraxial setup, similar to the deployment in Figure 2. This is obtained by setting $d_F = d_B = d$, $\theta_F = 0$, $\theta_B = \pi$, and $\psi_F = \psi_B = 0$. As for the focusing centres, we set $\mathbf{p}_{RB} = \mathbf{c}_B$ and $\mathbf{p}_{RF} = \mathbf{c}_U$, according to Section 4.2.

The results in Figure 4 confirm the effectiveness of the proposed approach, according to the theoretical analysis for this case study. In Figure 5, we consider a similar setup with $d = 7$ m, and compare the "Non-diagonal RIS" (ND-RIS)
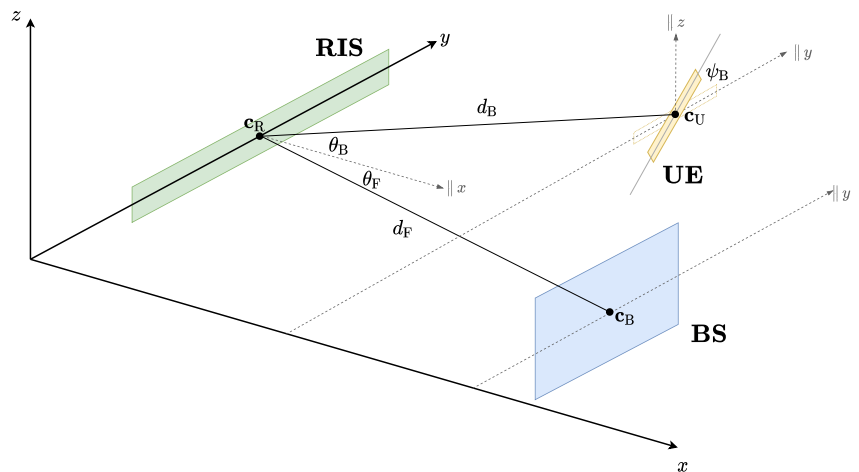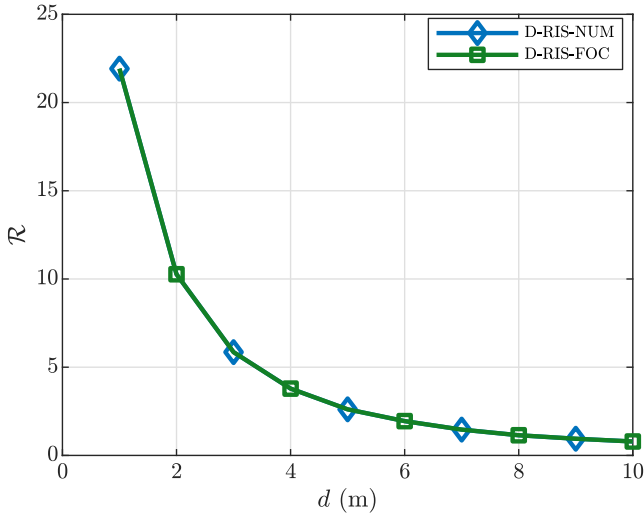

FIGURE 3 Considered network topology.

FIGURE 4 Achievable rate in the paraxial deployment – Comparison between the "Diagonal RIS - Numerical" (D-RIS-NUM) and "Diagonal RIS - Proposed" (D-RIS-FOC) schemes. Setup: $d_F = d_B = d$, $\theta_F = 0$, $\theta_B = \pi$, and $\psi_F = \psi_B = 0$.
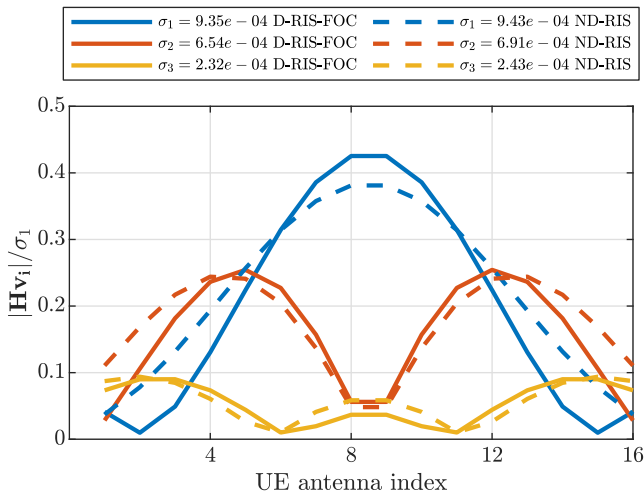

FIGURE 5 Achievable rate in the paraxial deployment – Beam projection, normalised by the highest singular value ($\sigma_1 = \sigma_{B1}\sigma_{F1}$), on the linear antenna array of the MIMO receiver: Comparison between the "Non-diagonal RIS" (ND-RIS) and "Diagonal RIS - Proposed" (D-RIS-FOC) schemes. Setup: $d_F = d_B = d = 7$ m, $\theta_F = 0$, $\theta_B = \pi$, and $\psi_F = \psi_B = 0$.

and "Diagonal RIS - Proposed" (D-RIS-FOC) schemes in terms of projected beams. For both schemes, specifically, we compute the matrix $\mathbf{V}_F \in \mathbb{C}^{N \times N}$ from the corresponding SVD, and we then compute the projections $\|\mathbf{H}\mathbf{v}_{Fi}\|$ with $\mathbf{v}_{Fi}$ being the ith vector in $\mathbf{V}_F$. This projection represents how the energy of the transmitted signal is distributed across the MIMO receiver. The profiles of the obtained beams closely match with each other. The minor differences are due to the fact that the transmission distances of all the antenna elements are not exactly the same, and the Fresnel approximation applied in [22] is less accurate in the considered near

field setup. Therefore, the focusing functions in Equation (23) and (24) constitute an approximation.
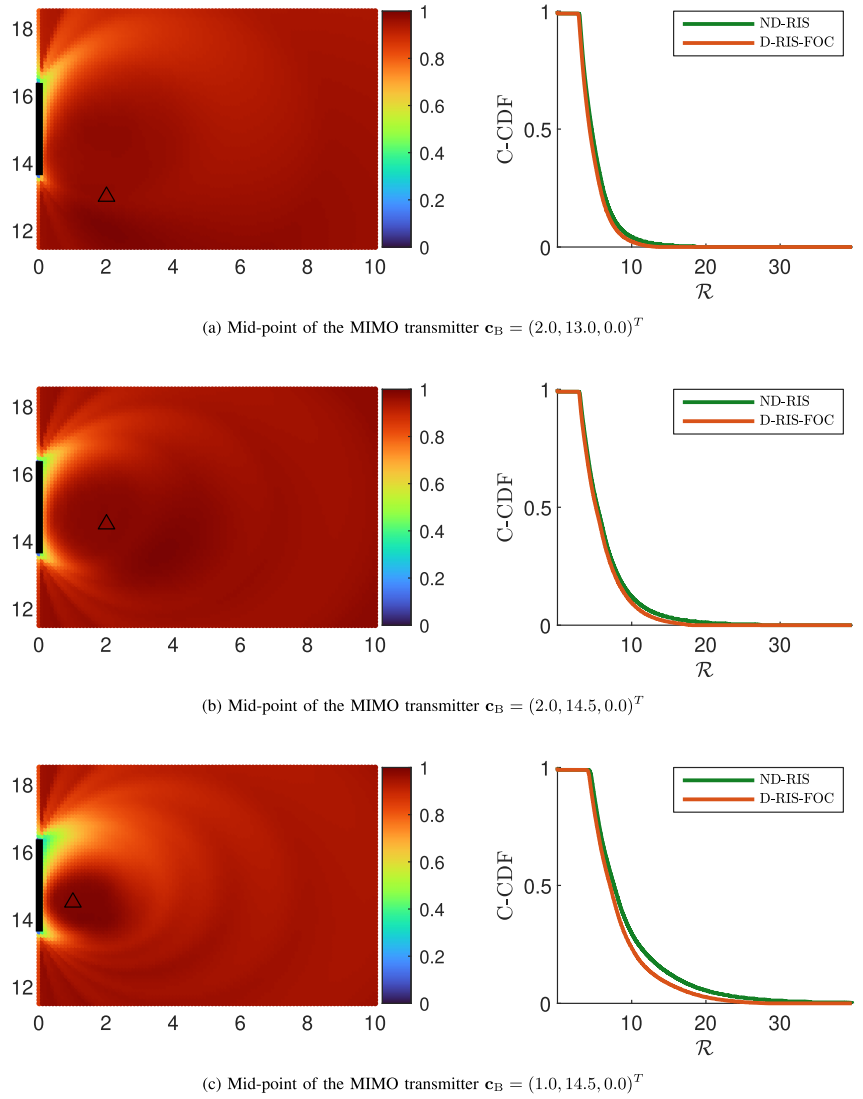
5.2 | Non-paraxial setup

In this sub-section, we analyse the effectiveness of the proposed approximated diagonal design for RIS in non-paraxial setups. To this end, we compute and compare the achievable rates and the effective rank [52] provided by the "Non-diagonal RIS" (ND-RIS) and "Diagonal RIS - Proposed" (D-RIS-FOC) schemes, as a function of the location of the MIMO receiver, while keeping the location of the MIMO transmitter fixed. The effective rank, in particular, provides information on the number of degrees of freedom that is achievable in the considered channel model.

In Figure 6, we show the ratio of the achievable rates between the "Diagonal RIS - Proposed" (D-RIS-FOC) and the "Non-diagonal RIS" (ND-RIS) schemes. By definition, the ratio lies in the range [0, 1], and the closer to one the ratio is the closer to the optimum the "Diagonal RIS - Proposed" (D-RIS-FOC) scheme is. The location of the MIMO transmitter is denoted by a black triangle, and the RIS is represented by a black segment. The MIMO transmitter, RIS, and MIMO receiver are assumed to be parallel to each other, that is, $\psi_F = \psi_B = 0$. We see that the proposed approach provides rates very close to the optimum, except for some locations that are very close to the RIS (within 1 m from the RIS). In addition, we show the complementary cumulative distribution function of the achievable rates across the considered areas. The obtained curves confirm the good performance offered by the "Diagonal RIS - Proposed" (D-RIS-FOC) scheme with respect to the optimum. As expected, the closer to the RIS the MIMO transmitter is, the better the rate is [36].

In Figure 7, we illustrate the effective rank provided by the "Diagonal RIS - Proposed" (D-RIS-FOC) scheme across the considered area. We see that multiple communication modes are available for different locations of the MIMO receiver, and the effective rank depends on the location of the MIMO transmitter. The obtained results confirm that the network topology and the locations of the MIMO transmitter, RIS, and MIMO receiver are essential parameters for ensuring multi-mode communications. Also, we compare the effective rank provided by the "Diagonal RIS - Proposed" (D-RIS-FOC) scheme against the "Non-diagonal RIS" (ND-RIS) scheme. We note that the proposed diagonal design, given in a closed-form expression, provides an effective rank that is close to the optimum, but at a lower implementation complexity.

In Figure 8, we compare the achievable rates of the three considered schemes as a function of $\theta_F = -\theta_B = \theta$, while keeping the distances $d_F = d_B = d$ fixed. Overall, we see that the proposed approach provides rates that are virtually identical to those obtained with complex numerical algorithms and slightly worse than those obtained by using non-diagonal RIS only in some cases.

FIGURE 6 (left) Ratio of the achievable rate between the "Diagonal RIS – Proposed" (D-RIS-FOC) and the "Non-diagonal RIS" (ND-RIS) schemes as a function of the position of the MIMO receiver (a given point on the colour map) for a fixed location of the MIMO transmitter. (right) Complementary cumulative distribution function (C-CDF) of the achievable rate for the "Non-diagonal RIS" (ND-RIS) and the "Diagonal RIS – Proposed" (D-RIS-FOC) schemes across the considered areas.

(a) Mid-point of the MIMO transmitter $\mathbf{c}_B = (2.0, 13.0, 0.0)^T$

(b) Mid-point of the MIMO transmitter $\mathbf{c}_B = (2.0, 14.5, 0.0)^T$

(c) Mid-point of the MIMO transmitter $\mathbf{c}_B = (1.0, 14.5, 0.0)^T$

In Figure 9, we compare the achievable rates offered by the considered three schemes as a function of the distance $d_B = d$, while keeping the other parameters fixed. The conclusions are similar to those drawn from the analysis of Figure 8.

In Figure 10, we compare the achievable rates offered by the considered schemes as a function of the rotation angle ψ_B and the focusing point $\mathbf{p}_{RF}$. The main objective is to understand the impact of rotating the receiver, which results in large deviations from the typical paraxial setup, and to evaluate the impact of the focusing points at the MIMO receiver, that is, whether choosing the mid-point as the focusing point, as dictated by the paraxial setup, is a good choice. The obtained results unveil two main performance trends: (1) Selecting the mid-point of the MIMO receiver as the focusing point is the best choice, as it provides rates that are very close to those obtained by using the "Diagonal RIS - Numerical" (D-RIS-NUM) scheme; and (2) rotating the MIMO receiver increases the gap between the rates attained by the "Diagonal RIS - Proposed" (D-RIS-FOC) scheme and the "Non-diagonal RIS"

(ND-RIS) scheme. In general, a non-diagonal design for RIS provides better rates in the presence of rotations.

5.3 | Water-filling versus uniform power allocation

In this sub-section, in order to further simplify the proposed design for RIS, we evaluate the achievable rate of the D-RIS-FOC scheme that is obtained by using the optimal power allocation strategy based on the water-filling against the uniform power allocation. The results are illustrated in Figures 11 and 12. Both figures are obtained by using the same methodology as for Figure 6.

Figure 11 shows the ratio of the achievable rates that is obtained by using the uniform and the water-filling power allocation strategies. It can be seen that the water-filling power allocation outperforms the uniform power allocation at any position of the receiver, especially when it is located far away
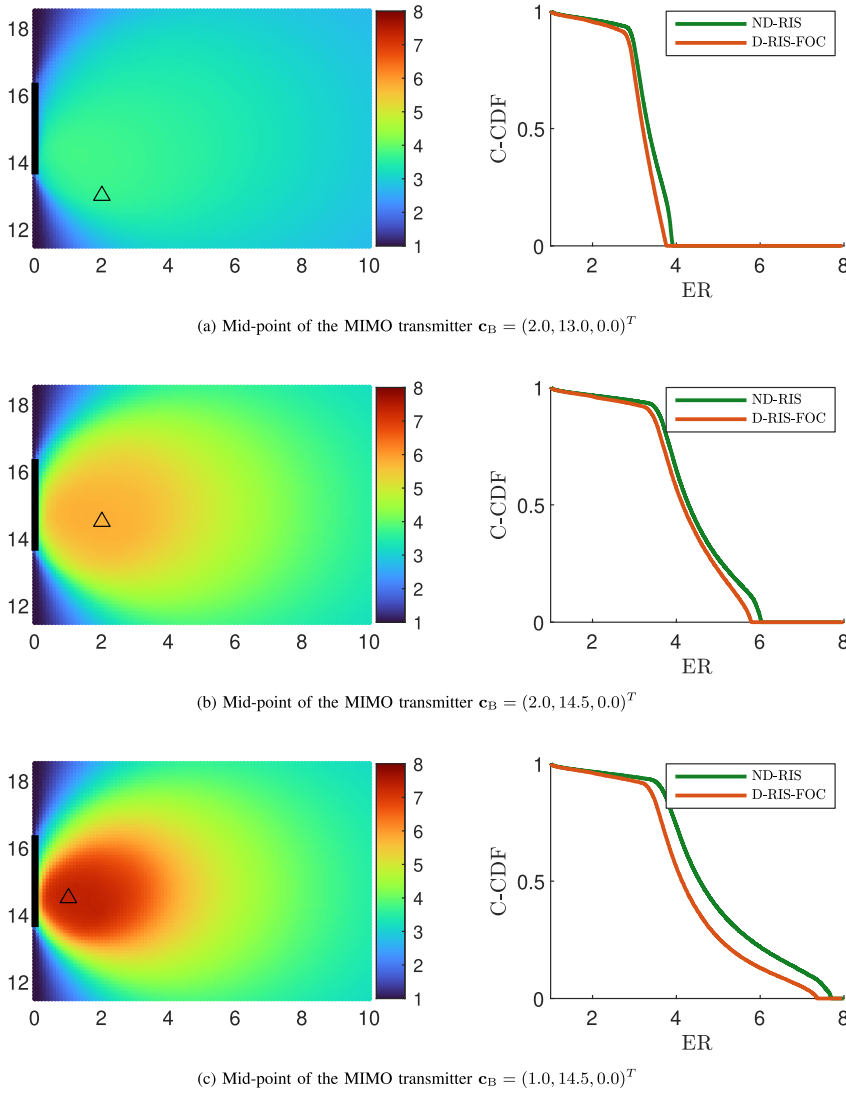
(a) Mid-point of the MIMO transmitter $\mathbf{c}_B = (2.0, 13.0, 0.0)^T$

(b) Mid-point of the MIMO transmitter $\mathbf{c}_B = (2.0, 14.5, 0.0)^T$

(c) Mid-point of the MIMO transmitter $\mathbf{c}_B = (1.0, 14.5, 0.0)^T$

FIGURE 7 (left) Effective rank (ER) of the "Diagonal RIS – Proposed" (D-RIS-FOC) scheme as a function of the position of the MIMO receiver (a given point on the colour map) for a fixed location of the MIMO transmitter. (right) C-CDF of the ER for the "Non-diagonal RIS" (ND-RIS) and the "Diagonal RIS – Proposed" (D-RIS-FOC) schemes across the considered areas.
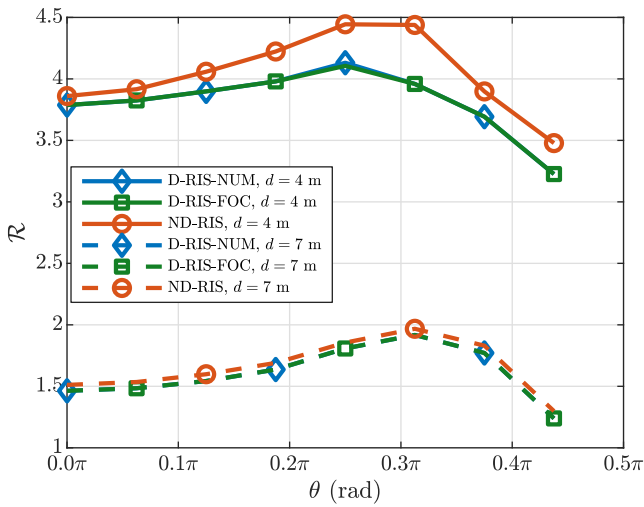

FIGURE 8 Comparison of the achievable rates offered by the "Non-diagonal RIS" (ND-RIS), "Diagonal RIS - Numerical" (D-RIS-NUM), and "Diagonal RIS - Proposed" (D-RIS-FOC) schemes as a function of the angle $\theta_F = -\theta_B = \theta$, while keeping the distances $d_F = d_B = d$ fixed (solid lines: $d = 4$ m; dashed lines: $d = 7$ m). The MIMO transmitter, RIS, and MIMO receiver are parallel to each other ($\psi_F = \psi_B = 0$).

from the RIS. Even considering locations of the receiver that are in the very close proximity of the RIS, the ratio between the rates is no greater than 0.7.

The comparison illustrated in Figure 11 may, however, not be fair. In fact, the uniform power allocation assumes that the same power is given to channels corresponding to very small singular values. For a fairer comparison, we consider the case study in which the uniform power allocation is applied only to the channels whose singular values are no smaller than 10 dB compared with the largest singular value. In other words, the uniform power allocation is applied to channels whose singular values fulfil the condition $\sigma_i > 0.1 \max\{\boldsymbol{\sigma}\}$. On the other hand, the power allocated to the channels that do not fulfil this condition is set equal to zero.

The results are illustrated in Figure 12. In this case, the uniform power allocation provides much better results. Specifically, we see that the ratio between the obtained rates unlikely falls below 0.8. This implies that the enhanced uniform power allocation provides rates that are similar to the water-filling power allocation, but at a lower computational complexity. Depending on the desired tradeoff between

performance and complexity, one may decide to utilise the water-filling power allocation strategy or the improved uniform power allocation strategy.

5.4 | Computational complexity

In this sub-section, we analyse and compare the computational complexities of the proposed schemes for optimising the RIS. The three considered optimization schemes (D-RIS-NUM, ND-RIS, and D-RIS-FOC) consist of two distinct steps: (a) the computation of the matrix $\mathbf{\Phi}$ containing the RIS reflection coefficients and (b) the computation of the

precoding, combining, and power allocation matrices. Specifically, the three considered approaches use the SVD of the RIS-aided end-to-end channel to determine the precoding
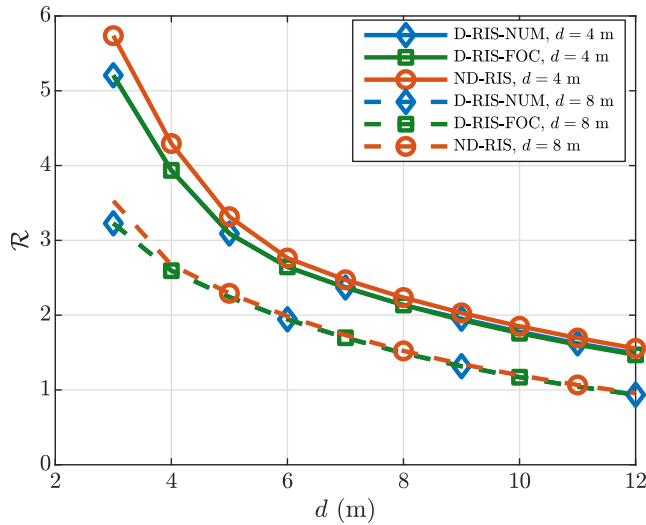

FIGURE 11 Water-filling versus equal power allocation: Ratio between the achievable rates obtained by using the uniform and the water-filling power allocation strategies.

FIGURE 12 Water-filling versus improved equal power allocation: Ratio between the achievable rates obtained by using the improved uniform and the water-filling power allocation strategies.

FIGURE 9 Comparison of the achievable rates offered by the "Non-diagonal RIS" (ND-RIS), "Diagonal RIS - Numerical" (D-RIS-NUM), and "Diagonal RIS - Proposed" (D-RIS-FOC) schemes as a function of the distance $d_B = d$, while keeping the distance d_F (solid lines: $d_F = 4$ m; dashed lines: $d_F = 8$ m), and the angles $\theta_F = \pi/8$ and $\theta_B = 3\pi/8$ fixed. The MIMO transmitter, RIS, and MIMO receiver are parallel to each other ($\psi_F = \psi_B = 0$).
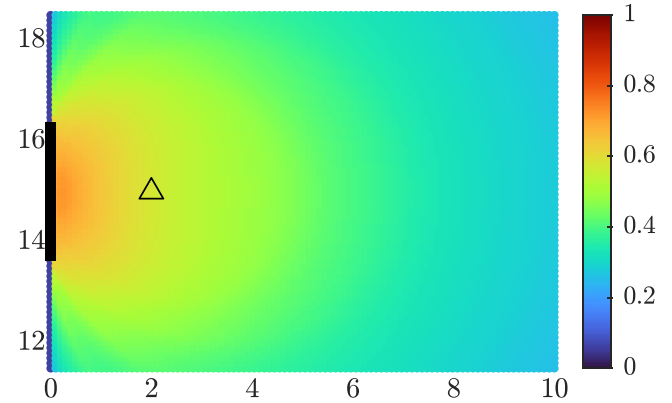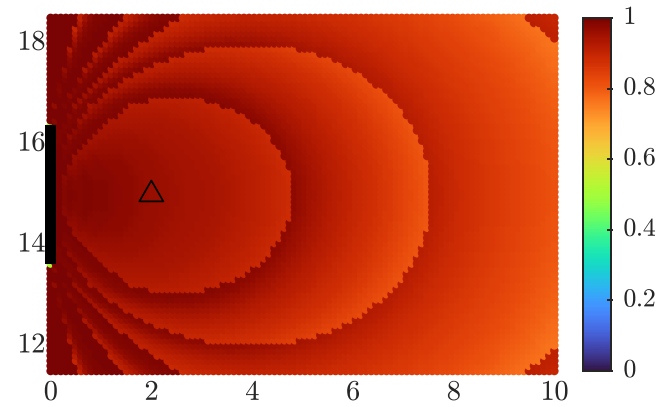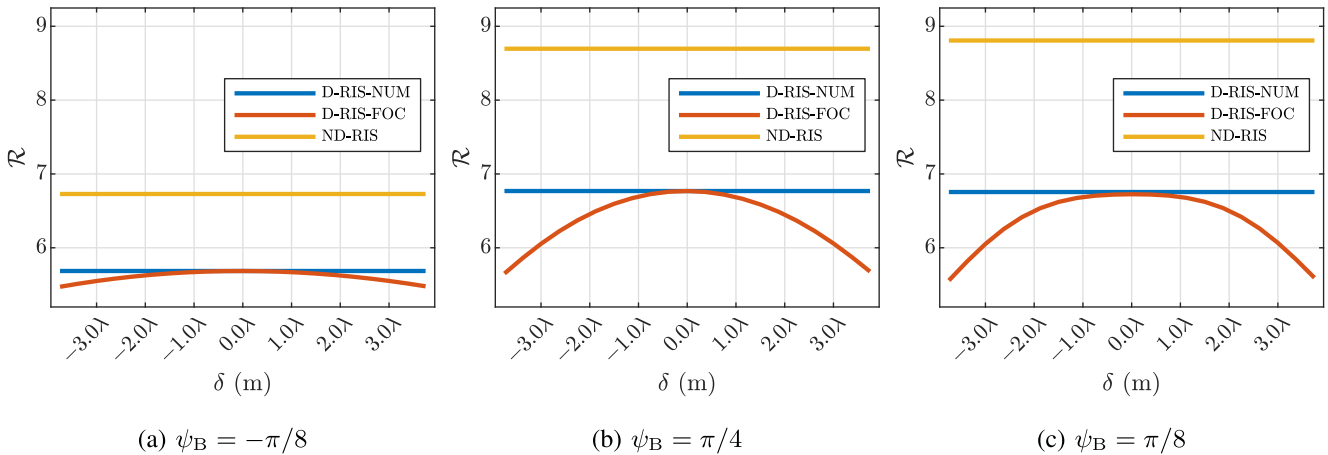

(a) $\psi_B = -\pi/8$ (b) $\psi_B = \pi/4$ (c) $\psi_B = \pi/8$

FIGURE 10 Comparison of the achievable rates offered by the "Non-diagonal RIS" (ND-RIS), "Diagonal RIS - Numerical" (D-RIS-NUM), and "Diagonal RIS - Proposed" (D-RIS-FOC) schemes as a function of the rotation angle ψ_B and the focusing point $\mathbf{p}_{RF}$. Specifically, $\mathbf{p}_{RF} = \delta \frac{\mathbf{u}_M - \mathbf{c}_U}{\|\mathbf{u}_M - \mathbf{c}_U\|}$, where $\mathbf{u}_M$ is the Mth element of the MIMO receiver. Setup: $\theta_F = \pi/4$, $\theta_B = \pi/3$, $d_F = 2$ m, $d_B = 3.5$ m, $\psi_F = 0$, and $\mathbf{p}_{RB} = \mathbf{c}_B$.

and decoding matrices, and the water-filling power allocation based on the singular values of the RIS-aided end-to-end channel. Since this step is the same for all the considered approaches, we disregard the associated computational complexity, with the caveat that, however, the SVD is computed multiple times for the D-RIS-NUM scheme, as it is based on an iterative algorithm. Hence, the computational complexity of the D-RIS-NUM scheme is underestimated in our analysis.

Therefore, we focus our attention only on the complexity of the first step, that is, the complexity of computing $\mathbf{\Phi}$, for each considered scheme.

- *Complexity of the D-RIS-NUM scheme*: In this case, the complexity is analysed in [49, Eq. (21)], where it is shown that it depends on the number K of RIS elements to the power of 3, that is, $\mathcal{O}(K^3)$.
- *Complexity of ND-RIS*: In this case, the computation of the SVD of both the forward $\mathbf{H}_F$ and backward $\mathbf{H}_B$ channels is needed. The complexity of computing the singular value decomposition of an n-by-m matrix is $\mathcal{O}(\min(m^2 n, n^2 m))$. Therefore, the complexity is linear with the number K of RIS elements, which is assumed to be larger than the number of antennas at the transmitter and receiver. Also, the method requires the computation of the product $\mathbf{V}_B \mathbf{U}_F^H$, whose complexity is $\mathcal{O}(K^{2.373})$ [53].
- *Complexity of D-RIS-FOC*: In this case, unlike the other two considered schemes, the matrix of RIS reflection coefficients is given in a closed-form expression and is obtained from the positions of the transmitter, RIS, and receiver. The complexity of this computation is linear with the number K of RIS elements, that is, it is $\mathcal{O}(K)$.

Therefore, the proposed D-RIS-FOC scheme provides the lowest complexity among the considered schemes.

6 | CONCLUSION

In this paper, we have analysed the spatial multiplexing gains of RIS-aided MIMO channels in the near field. We have proved that the best design for nearly-passive RIS results in a non-diagonal matrix of reflection coefficients. Due to the non-negligible complexity of non-diagonal designs for RIS, we have proposed a closed-form diagonal design that is motivated and is proved to be optimal, from the end-to-end channel capacity standpoint, in line-of-sight channels and when the MIMO transmitter, RIS, and MIMO receiver are deployed according to the paraxial setup. In different network topologies and over fading channels, the proposed design is sub-optimal. However, extensive simulation results in line-of-sight (free-space) channels have confirmed that it provides good performance in non-paraxial setups as well. Specifically, we have shown that the proposed diagonal design provides rates that are close to those obtained by numerically solving non-convex optimization problems at a high computational complexity, as well as to those attained, in several considered network setups,

by capacity-achieving non-diagonal RIS designs. Possible extensions of the proposed approach include the analysis of RIS-aided multi-user MIMO networks in line-of-sight and fading channels.

AUTHOR CONTRIBUTION

Giulio Bartoli: Investigation, Methodology, Validation, Writing – original draft, Writing – review & editing. **Andrea Abrardo**: Investigation, Methodology, Validation, Writing – original draft, Writing – review & editing. **Nicolo Decarli**: Investigation, Methodology, Validation, Writing – original draft, Writing – review & editing. **Davide Dardari**: Investigation, Methodology, Validation, Writing – original draft, Writing – review & editing. **Marco Di Renzo**: Investigation, Methodology, Validation, Writing – original draft, Writing – review & editing.

CONFLICT OF INTEREST STATEMENT

No conflict of interest.

DATA AVAILABILITY STATEMENT

Data available on request from the authors.

ORCID

Giulio Bartoli 🔟 https://orcid.org/0000-0003-1666-228X
Marco Di Renzo 🔟 https://orcid.org/0000-0003-0772-8793

REFERENCES

1. AI-Integrated Communications Use Case Release-1, Innovative Optical Wireless Network Global Forum. https://iowngf.org/wp-content/uploads/formidable/21/IOWN-GF-RD-AIC_Use_Case_1.0.pdf (2021)
2. European Telecommunications Standards Institute, Industry Specification Group on Terahertz. https://www.etsi.org/committee/2124-thz (2021)
3. Chen, Z., et al.: Terahertz wireless communications for 2030 and beyond: a cutting-edge frontier. IEEE Commun. Mag. 59(11), 66–72 (2021)
4. Han, C., et al.: Terahertz wireless channels: a holistic survey on measurement, modeling, and analysis. IEEE Commun. Surv. Tutor. 24(3), 1670–1707 (2022)
5. Chaccour, C., et al.: Can terahertz provide high-rate reliable low-latency communications for wireless VR? IEEE Internet Things J. 9(12), 9712–9729 (2022)
6. Akyildiz, I.F., Han, C., Nie, S.: Combating the distance problem in the millimeter wave and terahertz frequency bands. IEEE Commun. Mag. 56(6), 102–108 (2018)
7. Di Renzo, M., et al.: Reconfigurable intelligent surfaces vs. relaying: differences, similarities, and performance comparison. IEEE Open J. Commun. Soc. 1, 798–807 (2020)
8. European Commission Energy Efficiency Targets. https://energy.ec.europa.eu/topics/energy-efficiency/energy-efficiency-targets-directive-and-rules/energy-efficiency-targets_en (2022)

9. 3gpp tr 38.867 v1.0.0: Study on nr Network-Controlled Repeaters. https://portal.3gpp.org/desktopmodules/Specifications/Specification-Details.aspx?specificationId=3988 (2022)

10. Di Renzo, M., et al.: Smart radio environments empowered by reconfigurable intelligent surfaces: how it works, state of research, and the road ahead. IEEE J. Sel. Areas Commun. 38(11), 2450–2525 (2020)

11. Wu, Q., Zhang, R.: Towards smart and reconfigurable environment: intelligent reflecting surface aided wireless network. IEEE Commun. Mag. 58(1), 106–112 (2020)

12. Huang, C., et al.: Holographic MIMO surfaces for 6G wireless networks: opportunities, challenges, and trends. IEEE Wirel. Commun. 27(5), 118–125 (2020)

13. Dardari, D., Decarli, N.: Holographic communication using intelligent surfaces. IEEE Commun. Mag. 59(6), 35–41 (2021)

14. Di Renzo, M.: Reconfigurable Surfaces for Wireless Communications [online]. IEEE EuCAP (2023). https://doi.org/10.5281/zenodo.7430186

15. Flamini, R., et al.: Toward a heterogeneous smart electromagnetic environment for millimeter-wave communications: an industrial viewpoint. IEEE Trans. Antenn. Propag. 70(10), 8898–8910 (2022)

16. Sayeed, A., Behdad, N.: Continuous aperture phased MIMO: basic theory and applications. In: 2010 48th Annual Allerton Conference on Communication, Control, and Computing, pp. 1196–1203. Allerton (2010)

17. Sanguinetti, L., D'Amico, A.A., Debbah, M.: Wavenumber-division multiplexing in line-of-sight holographic MIMO communications. IEEE Trans. Wirel. Commun. 1 (2022) https://ieeexplore.ieee.org/stamp/stamp.jsp?arnumber=9906802

18. Di Renzo, M., Dardari, D., Decarli, N.: LoS MIMO-Arrays vs. LoS MIMO-Surfaces [online]. IEEE EuCAP (2023). https://arxiv.org/abs/2210.08616

19. European Telecommunications Standards Institute, Industry Specification Group on Reconfigurable Intelligent Surfaces. https://www.etsi.org/committee/1966-ris (2020)

20. Bøhagen, F., Orten, P., Øien, G.E.: Construction and capacity analysis of high-rank line-of-sight MIMO channels. In: IEEE Wireless Communications and Networking Conference, WCNC 2005, pp. 432–437. IEEE, New Orleans (2005)

21. Do, H., et al.: Terahertz line-of-sight MIMO communication: theory and practical challenges. IEEE Commun. Mag. 59(3), 104–109 (2021)

22. Miller, D.A.B.: Communicating with waves between volumes: evaluating orthogonal spatial channels and limits on coupling strengths. Appl. Opt. 39(11), 1681–1699 (2000)

23. Thaning, A., et al.: Limits of diffractive optics by communication modes. J. Opt. Pure Appl. Opt. 5(3), 153 (2003)

24. Dardari, D.: Communicating with large intelligent surfaces: fundamental limits and models. IEEE J. Sel. Areas Commun. 38(11), 2526–2537 (2020)

25. Tse, D., Viswanath, P.: Fundamentals of Wireless Communication. Cambridge University Press (2005)

26. Decarli, N., Dardari, D.: Communication modes with large intelligent surfaces in the near field. IEEE Access. 9, 165648–165666 (2021)

27. Pizzo, A., et al.: Nyquist sampling and degrees of freedom of electromagnetic fields. IEEE Trans. Signal Process. 70, 3935–3947 (2022)

28. Di Renzo, M., Galdi, V., Castaldi, G.: Modeling the Mutual Coupling of Reconfigurable Metaurfaces [online]. IEEE EuCAP (2023). https://arxiv.org/abs/2210.08619

29. El Mossallamy, M.A., et al.: Reconfigurable intelligent surfaces for wireless communications: principles, challenges, and opportunities. IEEE Trans. Cogn.e Commun. Netw. 6(3), 990–1002 (2020)

30. El Mossallamy, M.A., et al.: On spatial multiplexing using reconfigurable intelligent surfaces. IEEE Wireless Commun. Lett. 10(2), 226–230 (2021)

31. Zhang, S., Zhang, R.: Capacity characterization for intelligent reflecting surface aided MIMO communication. IEEE J. Sel. Areas Commun. 38(8), 1823–1838 (2020)

32. Perovic, N.S., et al.: Achievable rate optimization for MIMO systems with reconfigurable intelligent surfaces. IEEE Trans. Wirel. Commun. 20(6), 3865–3882 (2021)

33. Abrardo, A., et al.: MIMO interference channels assisted by reconfigurable intelligent surfaces: mutual coupling aware sum-rate optimization based on a mutual impedance channel model. IEEE Wirel. Commun. Lett. 10(12), 2624–2628 (2021)

34. Han, Y., et al.: Double-IRS aided MIMO communication under LoS channels: capacity maximization and scaling. IEEE Trans. Commun. 70(4), 2820–2837 (2022)

35. Zhou, W., et al.: Joint precoder, reflection coefficients, and equalizer design for IRS-assisted MIMO systems. IEEE Trans. Commun. 70(6), 4146–4161 (2022)

36. Perovic, N.S., et al.: On the achievable sum-rate of the RIS-aided MIMO broadcast channel. IEEE Trans. Sig. Process. (2023). https://arxiv.org/abs/2104.12108

37. Shen, S., Clerckx, B., Murch, R.D.: Modeling and architecture design of reconfigurable intelligent surfaces using scattering parameter network analysis. IEEE Trans. Wirel. Commun. 21(2), 1229–1243 (2022)

38. Li, Q., et al.: Reconfigurable intelligent surfaces relying on non-diagonal phase shift matrices. IEEE Trans. Veh. Technol. 71(6), 6367–6383 (2022)

39. Li, H., Shen, S., Clerckx, B.: Beyond diagonal reconfigurable intelligent surfaces: from transmitting and reflecting modes to single-, group-, and fully-connected architectures. IEEE Trans. Wireless Commun. 1 (2022)

40. Do, H., Lee, N., Lozano, A.: Line-of-sight MIMO via intelligent reflecting surface. IEEE Trans. Wireless Commun. 1 (2022)

41. Díaz-Rubio, A., et al.: From the generalized reflection law to the realization of perfect anomalous reflectors. Sci. Adv. 3(8), e1602714 (2017)

42. Di Renzo, M., Danufane, F.H., Tretyakov, S.A.: Communication models for reconfigurable intelligent surfaces: from surface electromagnetics to wireless networks optimization. Proc. IEEE. 110(9), 1164–1209 (2022)

43. Telatar, E.: Capacity of multi-antenna Gaussian channels. Eur. Trans. Telecommun. 10(6), 585–595 (1999)

44. Gradoni, G., Di Renzo, M.: End-to-end mutual coupling aware communication model for reconfigurable intelligent surfaces: an electromagnetic-compliant approach based on mutual impedances. IEEE Wirel. Commun. Lett. 10(5), 938–942 (2021)

45. Fang, Z., Hua, Y., Koshy, J.: Joint source and relay optimization for a non-regenerative MIMO relay. In: Fourth IEEE Workshop on Sensor Array and Multichannel Processing, 2006, pp. 239–243 (2006)

46. Tang, X., Hua, Y.: Optimal design of non-regenerative MIMO wireless relays. IEEE Trans. Wirel. Commun. 6(4), 1398–1407 (2007)

47. Zhang, H., et al.: Intelligent omni-surfaces for full-dimensional wireless communications: principles, technology, and implementation. IEEE Commun. Mag. 60(2), 39–45 (2022)

48. Slepian, D., Pollak, H.O.: Prolate spheroidal wave functions, Fourier analysis and uncertainty. Bell Syst. Techn. J. 40(1), 43–63 (1961)

49. Abrardo, A., Dardari, D., Di Renzo, M.: Intelligent reflecting surfaces: sum-rate optimization based on statistical position information. IEEE Trans. Commun. 69(10), 7121–7136 (2021)

50. Pan, C., et al.: An overview of signal processing techniques for RIS/IRS-aided wireless systems. IEEE J. Sel. Top. Signal Process. 16(5), 883–917 (2022)

51. Ruiz-Sicilia, J.C., et al.: On the Degrees of Freedom of RIS-Aided Holographic MIMO Systems [online]. IEEE WSA (2023). Available: https://arxiv.org/abs/2301.07968

52. Roy, O., Vetterli, M.: The effective rank: a measure of effective dimensionality. In: 15th European Signal Processing Conference, EUSIPCO 2007, Poznan, Poland, 3–7 September 2007, pp. 606–610. IEEE (2007).

53. Alman, J., Williams, V.V.: A refined laser method and faster matrix multiplication. In: Marx, D. (ed.) Proceedings of the 2021 ACM-SIAM Symposium on Discrete Algorithms, SODA 2021, Virtual Conference, 10–13 January 2021, pp. 522–539. SIAM (2021)

APPENDIX A

PROOF OF PROPOSITION 1

In this appendix, we provide a formal proof for Proposition 1. The proposed approach generalises, to RIS-aided MIMO channels, the proof originally given in [43] for MIMO channels. The proof leverages the assumption that the matrix of reflection coefficients of the RIS is unitary but is not necessarily diagonal. For ease of notation, we assume $\sigma_n^2 = 1$.

By definition, assuming that the channels are fixed and given, the mutual information is.

$$I(\mathbf{x}, \mathbf{y}) = \log \det\left(\mathbf{I}_M + \mathbf{H}\mathbf{Q}\mathbf{H}^\dagger\right) \tag{27}$$

$$= \log \det\left(\mathbf{I}_M + \mathbf{Q}\mathbf{H}^\dagger\mathbf{H}\right) \tag{28}$$

where the last equality follows by using the identity $\det(\mathbf{I} + \mathbf{A}\mathbf{B}) = \det(\mathbf{I} + \mathbf{B}\mathbf{A})$.

The channel product $\mathbf{H}^\dagger\mathbf{H}$ can be expressed as

$$\begin{aligned} \mathbf{H}^\dagger\mathbf{H} &= (\mathbf{H}_B\boldsymbol{\Phi}\mathbf{H}_F)^\dagger(\mathbf{H}_B\boldsymbol{\Phi}\mathbf{H}_F) \\ &= \left(\mathbf{H}_F^\dagger\boldsymbol{\Phi}^\dagger\mathbf{H}_B^\dagger\right)(\mathbf{H}_B\boldsymbol{\Phi}\mathbf{H}_F) \\ &= \left(\mathbf{U}_F\boldsymbol{\Sigma}_F\mathbf{V}_F^\dagger\right)^\dagger\boldsymbol{\Phi}^\dagger\left(\mathbf{V}_B\boldsymbol{\Sigma}_B^\dagger\boldsymbol{\Sigma}_B\mathbf{V}_B^\dagger\right)\boldsymbol{\Phi}\left(\mathbf{U}_F\boldsymbol{\Sigma}_F\mathbf{V}_F^\dagger\right) \end{aligned} \tag{29}$$

Similarly to [46], without loss of generality, we can express the matrix $\boldsymbol{\Phi}$ as

$$\boldsymbol{\Phi} = \mathbf{V}_B\mathbf{X}\mathbf{U}_F^\dagger \tag{30}$$

with $\mathbf{X}$ being a generic unitary matrix, not necessarily diagonal.

Therefore, the mutual information can be expressed as.

$$I(\mathbf{x}, \mathbf{y}) = \log \det\left(\mathbf{I}_M + \mathbf{Q}\mathbf{V}_F\boldsymbol{\Sigma}_F^\dagger\mathbf{X}^\dagger\boldsymbol{\Sigma}_B^\dagger\boldsymbol{\Sigma}_B\mathbf{X}\boldsymbol{\Sigma}_F\mathbf{V}_F^\dagger\right) \tag{31}$$

$$= \log \det\left(\mathbf{I}_M + \mathbf{V}_F^\dagger\mathbf{Q}\mathbf{V}_F\boldsymbol{\Sigma}_F^\dagger\mathbf{X}^\dagger\boldsymbol{\Sigma}_B^\dagger\boldsymbol{\Sigma}_B\mathbf{X}\boldsymbol{\Sigma}_F\right) \tag{32}$$

$$= \log \det\left(\mathbf{I}_M + \tilde{\mathbf{Q}}\tilde{\mathbf{X}}\right) \tag{33}$$

where the last equality is obtained by defining.

$$\tilde{\mathbf{Q}} = \mathbf{V}_F^\dagger\mathbf{Q}\mathbf{V}_F \tag{34}$$

$$\tilde{\mathbf{X}} = \boldsymbol{\Sigma}_F\mathbf{X}^\dagger\boldsymbol{\Sigma}_B\boldsymbol{\Sigma}_B\mathbf{X}\boldsymbol{\Sigma}_F \tag{35}$$

Let us focus on the matrix $\tilde{\mathbf{Q}}$. Since $\mathbf{V}_F$ is unitary, we have $\mathrm{tr}(\tilde{\mathbf{Q}}) = \mathrm{tr}(\mathbf{Q})$. Therefore, maximising over $\mathbf{Q}$ is equivalent to maximising over $\tilde{\mathbf{Q}}$, without changing any constraints of the original optimization problem, since $\tilde{\mathbf{Q}}$ is positive semi-definite if $\mathbf{Q}$ is positive semi-definite. This is proven in the following lemma.

Lemma 1 *Matrix $\tilde{\mathbf{Q}}$ is positive semi-definite.*

Proof This lemma can be proven by observing the following.

- $\tilde{\mathbf{Q}}$ is an Hermitian matrix, since

$$\tilde{\mathbf{Q}}^\dagger = \left(\mathbf{V}_F^\dagger\mathbf{Q}\mathbf{V}_F\right)^\dagger = \mathbf{V}_F^\dagger\mathbf{Q}\mathbf{V}_F = \tilde{\mathbf{Q}} \tag{36}$$

- As $\tilde{\mathbf{Q}}$ is an Hermitian matrix, it is positive semi-definite if $\mathbf{z}^\dagger\tilde{\mathbf{Q}}\mathbf{z} \geq 0$ for any complex vector $\mathbf{z}$. This follows because

$$\mathbf{z}^\dagger\tilde{\mathbf{Q}}\mathbf{z} = \mathbf{z}^\dagger\mathbf{V}_F^\dagger\mathbf{Q}\mathbf{V}_F\mathbf{z} = \tilde{\mathbf{z}}^\dagger\mathbf{Q}\tilde{\mathbf{z}} \geq 0 \tag{37}$$

where the last inequality follows because $\mathbf{Q}$ is positive semi-definite and $\tilde{\mathbf{x}} = \mathbf{V}_F\mathbf{z}$ is a generic complex vector.
This completes the proof. □

The mutual information can be rewritten as

$$\begin{aligned} I(\mathbf{x}, \mathbf{y}) &= \log \det\left(\mathbf{I}_M + \boldsymbol{\Sigma}_F\mathbf{V}_F^\dagger\mathbf{Q}\mathbf{V}_F\boldsymbol{\Sigma}_F^\dagger\mathbf{X}^\dagger\boldsymbol{\Sigma}_B^\dagger\boldsymbol{\Sigma}_B\mathbf{X}\right) \\ &= \log \det\left(\mathbf{I}_M + \overline{\mathbf{Q}}\,\overline{\mathbf{X}}\right) \end{aligned} \tag{38}$$

where the last equality is obtained by defining.

$$\overline{\mathbf{Q}} = \boldsymbol{\Sigma}_F\mathbf{V}_F^\dagger\mathbf{Q}\mathbf{V}_F\boldsymbol{\Sigma}_F^\dagger = \boldsymbol{\Sigma}_F\tilde{\mathbf{Q}}\boldsymbol{\Sigma}_F^\dagger \tag{39}$$

$$\overline{\mathbf{X}} = \mathbf{X}^\dagger\boldsymbol{\Sigma}_B^\dagger\boldsymbol{\Sigma}_B\mathbf{X} \tag{40}$$

Let us consider the matrix $\overline{\mathbf{X}}$. It can rewritten as

$$\begin{aligned} \overline{\mathbf{X}} &= \mathbf{X}^\dagger\tilde{\boldsymbol{\Sigma}}_B\mathbf{X} \\ &= \left(\tilde{\boldsymbol{\Sigma}}_B^{1/2}\mathbf{X}\right)^\dagger\left(\tilde{\boldsymbol{\Sigma}}_B^{1/2}\mathbf{X}\right) \end{aligned} \tag{41}$$

where $\tilde{\boldsymbol{\Sigma}}_B = \boldsymbol{\Sigma}_B^\dagger\boldsymbol{\Sigma}_B$ is a square diagonal matrix with non-negative real entries on its diagonal. The last equality follows because the matrix $\tilde{\boldsymbol{\Sigma}}_B$ is invertible and can written as $\tilde{\boldsymbol{\Sigma}}_B = \boldsymbol{\Sigma}_B^{1/2}\boldsymbol{\Sigma}_B^{1/2}$. Also, the last equality implies that $\overline{\mathbf{X}}$ is a positive semi-definite matrix for any choice of $\mathbf{X}$.

Accordingly, $\overline{\mathbf{X}}$ can be expressed in terms of its eigenvalue decomposition as $\overline{\mathbf{X}} = \mathbf{U}_{\overline{\mathbf{X}}}\boldsymbol{\Lambda}_{\overline{\mathbf{X}}}\mathbf{U}_{\overline{\mathbf{X}}}^\dagger$. As a result, the mutual information can be rewritten as

$$\begin{aligned} I(\mathbf{x}, \mathbf{y}) &= \log \det\left(\mathbf{I}_M + \overline{\mathbf{Q}}\left(\mathbf{U}_{\overline{\mathbf{X}}}\boldsymbol{\Lambda}_{\overline{\mathbf{X}}}\mathbf{U}_{\overline{\mathbf{X}}}^\dagger\right)\right) \\ &= \log \det\left(\mathbf{I}_M + \boldsymbol{\Lambda}_{\overline{\mathbf{X}}}^{1/2}\mathbf{U}_{\overline{\mathbf{X}}}^\dagger\overline{\mathbf{Q}}\mathbf{U}_{\overline{\mathbf{X}}}\boldsymbol{\Lambda}_{\overline{\mathbf{X}}}^{1/2}\right) \end{aligned} \tag{42}$$

From Equation (39) and (42), the following considerations can be made.

- The matrix $\overline{\mathbf{Q}} = \boldsymbol{\Sigma}_F\tilde{\mathbf{Q}}\boldsymbol{\Sigma}_F^\dagger$ is positive semi-definite, since $\tilde{\mathbf{Q}}$ is positive semi-definite. The proof is the same as for Lemma 1.

- The matrix $\mathbf{U}_{\overline{\mathbf{X}}}^{\dagger}\overline{\mathbf{Q}}\mathbf{U}_{\overline{\mathbf{X}}}$ is positive semi-definite, since $\overline{\mathbf{Q}}$ is positive semi-definite. The proof is the same as for Lemma 1.

- The matrix $\mathbf{\Lambda}_{\overline{\mathbf{X}}}^{1/2}\mathbf{U}_{\overline{\mathbf{X}}}^{\dagger}\overline{\mathbf{Q}}\mathbf{U}_{\overline{\mathbf{X}}}\mathbf{\Lambda}_{\overline{\mathbf{X}}}^{1/2}$ is positive semi-definite, since $\mathbf{U}_{\overline{\mathbf{X}}}^{\dagger}\overline{\mathbf{Q}}\mathbf{U}_{\overline{\mathbf{X}}}$ is positive semi-definite. The proof is the same as for Lemma 1.

Therefore, the matrix $\mathbf{I}_M + \mathbf{\Lambda}_{\overline{\mathbf{X}}}^{-1/2}\mathbf{U}_{\overline{\mathbf{X}}}^{\dagger}\overline{\mathbf{Q}}\mathbf{U}_{\overline{\mathbf{X}}}\mathbf{\Lambda}_{\overline{\mathbf{X}}}^{-1/2}$ is positive semi-definite as well. From [43], it is known that, for any generic positive semi-definite matrix $\mathbf{A}$ (therein referred to as non-negative defined), we have

$$\det(\mathbf{A}) \leq \prod_i \mathbf{A}(i,i) = \prod_i (\mathbf{A})_{i,i} \qquad (43)$$

where the notation $\mathbf{A}(i,i) = (\mathbf{A})_{i,i}$ is employed to simplify the writing.

Let us consider the formulation of the mutual information in Equation (33), which is the most convenient one for further analysis. By using the upper-bound in Equation (43), we obtain

$$\begin{aligned}
I(\mathbf{x},\mathbf{y}) &= \log \det(\mathbf{I}_M + \tilde{\mathbf{Q}}\tilde{\mathbf{X}}) \\
&\leq \log \prod_i (\mathbf{I}_M + \tilde{\mathbf{Q}}\tilde{\mathbf{X}})_{ii}
\end{aligned} \qquad (44)$$

Based on [43], a sufficient condition to attain the upper-bound, that is, (44) is fulfiled with equality, is that $\tilde{\mathbf{X}}$ and $\tilde{\mathbf{Q}}$ are two diagonal matrices. Under these assumptions, we obtain

$$\begin{aligned}
I(\mathbf{x},\mathbf{y}) &= \log \prod_i (\mathbf{I}_M + \tilde{\mathbf{Q}}\tilde{\mathbf{X}})_{ii} \\
&= \log \prod_i (\mathbf{I}_M + \tilde{\mathbf{Q}}\mathbf{\Sigma}_{\mathrm{F}}\mathbf{X}^{\dagger}\mathbf{\Sigma}_{\mathrm{B}}\mathbf{\Sigma}_{\mathrm{B}}\mathbf{X}\mathbf{\Sigma}_{\mathrm{F}})_{ii} \\
&= \log \prod_i (1 + \tilde{\mathbf{Q}}(i,i)\sigma_{\mathrm{F}i}\mathbf{X}^{\dagger}(i,i)\sigma_{\mathrm{B}i}\sigma_{\mathrm{B}i}\mathbf{X}(i,i)\sigma_{\mathrm{F}i}) \\
&= \log \prod_i (1 + \sigma_{\mathrm{B}i}^2\sigma_{\mathrm{F}i}^2\tilde{\mathbf{Q}}(i,i))
\end{aligned}$$
$$(45)$$

where the last equality follows because $\mathbf{X}^{\dagger}(i,i)\mathbf{X}(i,i) = 1$, since $\mathbf{X}$ is a unitary and diagonal if $\tilde{\mathbf{X}}$ is diagonal for achieving the upper-bound.

In summary, we have proved that $\tilde{\mathbf{Q}} = \mathbf{V}_{\mathrm{F}}^{\dagger}\mathbf{Q}\mathbf{V}_{\mathrm{F}}$ and that $\mathbf{\Phi} = \mathbf{V}_{\mathrm{B}}\mathbf{X}\mathbf{U}_{\mathrm{F}}^{\dagger}$, for any unitary and diagonal matrix $\mathbf{X}$, is capacity-achieving. Without loss of generality, therefore, we can consider $\mathbf{X} = \mathbf{I}_K$. The proof follows by noting that the capacity is achieved by applying the water-filling power allocation to the ordered product of the singular values of the transmitter-RIS and RIS-receiver channels.